Environmental Pollution 390 (2026) 127510

Contents lists available at ScienceDirect

Environmental Pollution

journal homepage: www.elsevier.com/locate/envpol

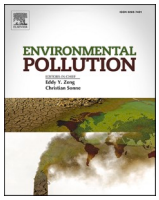

Indoor PM_{10} from fireplace, wood- and coal stove: morphology, composition, and oxidative potential in real residential settings☆

Estela D. Vicente [a,*], Isabella Charres [a], Yago Cipoli [a], Ana I. Calvo [b], Roberto Fraile [b], Carla Candeias [c], Fernando Rocha [c], Nuria Galindo [d], Eduardo Yubero [d], Célia Alves [a]

[a] Centre for Environmental and Marine Studies (CESAM), Department of Environment, University of Aveiro, 3810-193, Aveiro, Portugal
[b] Department of Physics, University of León, León, 24071, Spain
[c] Department of Geosciences, Geobiosciences, Geotechnologies and Geoengineering Research Centre (GeoBioTec), University of Aveiro, 3810-193, Aveiro, Portugal
[d] Atmospheric Pollution Laboratory (LCA), Department of Applied Physics, Miguel Hernandez University, Avenida de la Universidad S/N, 03202, Elche, Spain

ARTICLE INFO

Keywords:
Combustion appliance
Indoor air quality
Dithiothreitol assay
Ascorbic acid assay
Redox-active species

ABSTRACT

Residential combustion of solid fuels is a dominant source of indoor particulate matter (PM), with significant implications for human health. This study investigates the physicochemical properties and oxidative potential (OP) of indoor PM_{10} generated during the operation of different combustion appliances (woodstove, fireplace and coal stove) and fuels in real residential settings. Indoor and concurrent outdoor samples were analysed for water-soluble organic carbon (WSOC), elemental composition, particle morphology, and OP using both dithiothreitol (DTT) and ascorbic acid (AA) assays. Biomass combustion, especially in the fireplace, resulted in the highest indoor PM_{10}, OC, and WSOC levels, with WSOC/OC ratios reaching up to 0.84, suggesting a large contribution from oxygenated organics. Morphological analysis by SEM-EDS revealed a mixture of carbonaceous soot, mineral ash, and spherical fly ash particles, with clear fuel dependence. Elemental analysis showed higher Ca, Cl, K, S and Mn concentrations during woodstove combustion, while indoor samples from coal burning displayed lower levels for most elements. The OP_V of indoor samples was consistently higher during wood combustion compared with coal or background air, showing significant correlations with OC, WSOC, and potassium.

1. Introduction

Particulate matter (PM) is a major air pollutant with serious health and environmental consequences (Kelly and Fussell, 2015; Kim et al., 2015; Mukherjee and Agrawal, 2017). Despite global efforts to transition to cleaner energy, residential combustion of solid fuels (coal and biomass) remains widespread, representing a significant source of PM pollution (Jiang et al., 2024; Klimont et al., 2017; Leoni et al., 2018; Lin et al., 2019; Schwarz et al., 2019; Smołka-Danielowska et al., 2021; Weagle et al., 2018).

The incomplete combustion of solid fuels generates a complex mixture of airborne particles containing carbonaceous materials and a variety of organic and inorganic compounds. The physicochemical properties and toxicity of these emissions are influenced by multiple factors, including fuel type, combustion conditions, and stove technology (Kuye and Kumar, 2023; Vicente et al., 2024b; Vicente and Alves, 2018). Studies have demonstrated that emissions from different coal types and biomass fuels exhibit distinct compositional and morphological characteristics. For example, Zhang et al. (2018) found that lower-maturity coals emitted predominantly soot-organic matter particles during the flaming stage, whereas medium-maturity coals produced more abundant organic matter (OM) particles, and higher-maturity coals (e.g., anthracite and natural coke) generated mainly organic matter–sulphur (OM-S) particles. Overall carbon emissions decreased as coal maturity increased, as a result of both the intrinsic coal properties and higher burning temperatures, which favoured the formation of inorganic species (e.g., sulphates and other soluble ions) over carbonaceous particles. Similarly, Liu et al. (2017) reported that PM emissions from biomass combustion displayed phase-dependent variability, with softwood burning producing mainly OM particles in the smouldering phase, while hardwood combustion was characterised by soot-dominated emissions. The morphology of particulate matter,

☆ This paper has been recommended for acceptance by YING GUO.

* Corresponding author.
E-mail address: estelaavicente@ua.pt (E.D. Vicente).

https://doi.org/10.1016/j.envpol.2025.127510
Received 18 October 2025; Received in revised form 4 December 2025; Accepted 7 December 2025
Available online 8 December 2025

including shape, surface texture, and structure, plays a critical role in determining its toxicity and associated health effects. Irregular, elongated, or sharp-edged particles are more difficult for alveolar macrophages to clear, often resulting in cellular damage, persistent inflammation, and the development of respiratory diseases (Shangguan et al., 2024). The morphology is also key to identify the origin of the particles, as shown by Maher et al. (2016), who identified two distinct types of magnetite nanoparticles in human brain tissue: spherical particles with fused textures linked to anthropogenic (combustion-derived) sources, and angular, euhedral particles of biological origin. According to Maher et al. (2016), airborne magnetite particles with a diameter less than 200 nm can enter the body through the olfactory nerve and penetrate the brain. Due to their unique combination of redox activity, surface charge, and strong magnetic behaviour, these nanoparticles could contribute to the development of neurodegenerative diseases such as Alzheimer's. The physical and chemical characteristics of PM, including morphology and surface composition, play a crucial role in determining its interactions with biological systems and overall toxic behaviour.

One of the primary mechanisms linking PM exposure to adverse health outcomes is oxidative stress, which occurs when reactive oxygen species (ROS) overwhelm the body's antioxidant defences, leading to cellular damage and inflammation (Gurjar et al., 2010; Li et al., 2003). Particulate matter contributes to this imbalance either by generating ROS on its surfaces or through interactions with cells (Knaapen et al., 2004; Mazzoli-Rocha et al., 2010). Although antioxidant enzymes can help mitigate oxidative stress, an insufficient response can lead to cellular damage, affecting DNA, lipids, and proteins. This process is linked to inflammation and the development of respiratory and cardiovascular diseases, including asthma, chronic obstructive pulmonary disease, emphysema, and heart conditions (Peixoto et al., 2017). The oxidative potential (OP) of PM, a measure of its capacity to generate ROS, has emerged as a key indicator of PM toxicity and a valuable metric for assessing health risks (Bates et al., 2019; Gao et al., 2020; He and Zhang, 2023; Øvrevik, 2019).

Various methods have been developed to evaluate the OP of PM, including both cellular and acellular assays (Bates et al., 2019; Gao et al., 2020; He and Zhang, 2023; Vaccarella et al., 2025; Vicente et al., 2024b). Cellular assays, such as electron spin resonance (ESR) and fluorescence-based methods, assess ROS production in biological environments, while acellular assays quantify the depletion of antioxidants such as ascorbic acid (AA), glutathione (GSH), and dithiothreitol (DTT) upon exposure to PM (Bates et al., 2019; Gao et al., 2020; Vaccarella et al., 2025; Vicente et al., 2024b). Acellular assays are widely adopted for their speed, cost-efficiency, and reproducibility, enabling large-scale assessments of the OP across diverse environmental settings. Their application has proven valuable in source apportionment and epidemiological contexts (Bates et al., 2019; Gao et al., 2020; Vaccarella et al., 2025). The use of multiple OP assays provides complementary insights into PM toxicity, highlighting the importance of accounting for assay-specific sensitivities in health impact assessments (Gao et al., 2020; Janssen et al., 2014). Among the various acellular assays used to assess the OP of PM, the DTT assay is particularly responsive to organic compounds and redox-active metals such as copper and manganese. On the other hand, the AA and GSH assays are more sensitive to the presence of metals, especially iron and copper (Bates et al., 2019; Gao et al., 2020). The high OP of PM is often attributed to its complex chemical composition, which typically includes transition metals, organic compounds, and black carbon (Brehmer et al., 2019; Li et al., 2019b; Verma et al., 2015). Water-soluble organic carbon (WSOC) has emerged as a key contributor to the oxidative activity of PM, exhibiting strong correlations with OP responses, such as those measured by the DTT and AA assays (Gao et al., 2020; Verma et al., 2012).

To date, most studies investigating the OP of particles emitted from residential solid fuel combustion through acellular methods have focused primarily on characterising emissions (Cao et al., 2021; Isenor et al., 2024; Li et al., 2019b; Utinger et al., 2025; Zhang et al., 2024b) rather than the indoor PM to which residents are directly exposed during appliance operation. Existing research has been conducted in China and India, where solid fuel combustion is predominantly used for cooking rather than heating (Brehmer et al., 2019; Sharma et al., 2024). These studies generally examine fuel-burning cookstoves situated in semi-enclosed or outdoor kitchens, conditions that differ markedly from European residential settings in terms of appliance design, fuel characteristics, building characteristics, and ventilation. In Alaska, Yang et al. (2024) compared the OP of indoor PM generated from pellet combustion with that from other common household activities (e.g., cooking, incense burning). Overall, studies examining the OP of indoor particles originating specifically from residential solid fuel combustion remain scarce, and virtually no work has addressed this issue within European homes, where the context of solid fuel use, and thus potential exposure pathways, differs substantially. This gap highlights a critical need for regionally relevant indoor exposure assessments to better understand potential health risks associated with solid fuel heating in Europe.

The present study aims to investigate the morphological and chemical characteristics of PM_{10} particles released during residential coal and wood combustion, as well as their OP. By comparing indoor and outdoor samples, as well as combustion and non-combustion periods (background), this study provides valuable insights into the contribution of residential heating to indoor PM levels and their potential to induce oxidative stress.

2. Methodology

2.1. Sampling of PM_{10}

PM_{10} sampling campaigns were conducted in uninhabited residential houses under controlled combustion conditions, focusing on coal and wood as fuel sources. Details about the combustion appliances and fuels employed can be found in the supplementary material (Table S1, Fig. S1). During the mineral coal-burning campaign, experiments took place in a detached house, where PM_{10} samples were collected indoors, specifically in an open-plan kitchen/living area. The combustion process involved burning coal using a small-scale stand-alone stove over a 5-day period. The combustion cycle started by igniting newspaper sheets and wood chips, followed by six batches of coal, with consistent intervals between refuelling.

The wood-burning campaign was carried out in two uninhabited houses, each equipped with a different heating appliance: an open fireplace and a cast iron woodstove, both located in the kitchen area. The combustion cycles used a mixture of pine and eucalypt logs, with the fireplace being refuelled three times and the woodstove five times. The wood bed was periodically stirred to maintain a hot charcoal base.

All experiments were designed to replicate real-world practices, including ignition procedures, fire management, and the typical daily combustion duration. The experiments lasted approximately 6 h 40 min for coal and 8 h for biomass. They were conducted under minimum ventilation conditions, with all doors and windows closed. Details about the experimental conditions can be found in the supplementary material (Table S2). Background PM_{10} levels were monitored in each house when the combustion appliances were not in use to assess baseline air quality. In both campaigns, indoor and outdoor PM_{10} samples were collected concurrently, with high-volume samplers (MCV, model CAV-A/mb) operating at a flow rate of 30 $m^3\ h^{-1}$. The quartz-fibre filters were pre-weighed and conditioned for 48 h in a controlled environment ($T = 20\ ^\circ C \pm 1\ ^\circ C$, HR = 50 %) before and after sampling to ensure accurate gravimetric quantification.

2.2. Morphological and chemical characterisation of PM_{10}

The carbonaceous components of PM_{10} were quantified using a thermo-optical transmission method, which enables the separation of

organic carbon (OC) and elemental carbon (EC). Circular punches from the collected filters were subjected to a temperature-controlled protocol: under 100 % N_2, at the samples were heated at 150 °C for 4 min, at 350 °C for 4 min, at 600 °C for 5 min, and from 600 to 250 °C within 3 min. Subsequently, under a 96 % N_2/4 % O_2 atmosphere, the temperature was set at 350 °C for 1 min, from 350 to 500 °C within 7 min, and at 850 °C for 6 min. In the first atmosphere of pure nitrogen the OC thermally evolved and then, the EC was oxidised (O_2/N_2 atmosphere). The carbon released during each stage was converted to CO_2 and quantified using a non-dispersive infrared analyser. A detailed description of the method and results can be found in previous works (Vicente et al., 2024a; Vicente et al., 2020). Based on the variability observed across blank filter batches, the limit of detection for OC, defined as three times the standard deviation, was determined to be on the order of 30–80 ng m^{-3}. Evaluation of the thermograms indicates that carbon masses below 1 μg cannot be reliably quantified with the applied methodology when particle loading on the filters is low. This corresponds to a detection limit of approximately 30 ng m^{-3} for EC.

WSOC was extracted from the filters via ultrasonic agitation in ultrapure water, followed by analysis using a TOC-L CSH analyser (Shimadzu), which operates based on high-temperature catalytic oxidation at 680 °C. WSOC was measured as non-purgeable OC. For this determination, the aqueous extracts were acidified with 1 M hydrochloric acid (PanReac AppliChem), to remove inorganic carbon that would interfere with the WSOC measurement and purged with ultrapure air to remove volatile organic compounds and dissolved inorganic carbon. Each extract was analysed in triplicate, and the mean value was reported. Calibration was carried out using a standard solution of potassium hydrogen phthalate (PanReac AppliChem), and quality control was ensured through the inclusion of procedural blanks in every batch (Gómez-Sánchez et al., 2024). The detection limit of WSOC, defined as three times the standard deviation of blank filters, was 0.3 μg C m^{-3}. Measurement precision, assessed through a repeatability test (N = 16) using standard solutions, was better than 8 %. For quality assurance, a standard solution was analysed in triplicate after every 10 samples.

The elemental composition of PM_{10} samples was determined by energy-dispersive X-ray fluorescence (ED-XRF) using an ARL Quant'x spectrometer (Thermo Fisher Scientific, UK) equipped with a Peltier-cooled Si(Li) detector. Elemental excitation was achieved via an air-cooled Rh-anode X-ray tube, operated under five optimised conditions using different beam filters and voltages to enhance sensitivity for various element groups. Measurements were conducted under vacuum. Calibration was performed with Micromatter thin film standards and periodically verified using the NIST SRM2783 standard. Spectral deconvolution was carried out using WinTrace software (Thermo Electron Corp.) (Chiari et al., 2018). The detection limit for each element on quartz fibre filters was calculated as three times the standard deviation of the element concentrations measured in at least six different field blanks. The method detection limits for individual elements ranged from a few ng m^{-3} to several tens of ng for light elements. The repeatability was better than 5 % for standards and better than 10 % for PM_{10} filters. Further details can be found in previous publications (Chiari et al., 2018; Unga et al., 2025).

For a detailed analysis of particle morphology and size at the individual level, two 5 mm diameter punches were extracted from each quartz filter and subjected to analysis using a Tescan scanning electron microscope (SEM, model VEGA LMU). This equipment is capable of operating in both high and low vacuum conditions and is equipped with secondary and back-diffused electron detectors to capture high-resolution images. Additionally, an Energy Dispersive Spectrometer (EDS) was employed for semi-quantitative chemical characterisation. To identify inorganic particles individually, the protocols proposed by Wu et al. (2016) were followed.

2.3. Oxidative potential analysis

Two 9 mm diameter punches were taken from each sample and immersed in 12 mL of Milli-Q water. The samples were then extracted in an ultrasonic bath for a total of 30 min. The extracts were filtered using PVDF syringe 0.2 μm pore size filters (Whatman™) and analysed immediately. The OP of the PM_{10} water extracts was assessed using the AA and DTT assays, as described by Gómez-Sánchez et al. (2024).

For the AA assay, 1.5 ml of the sample extract was combined with 1.35 ml of 0.1 M potassium phosphate buffer (pH 7.4) and 150 μl of 2 mM ascorbic acid and incubated at 37 °C. The absorbance at 265 nm was measured at 15, 30, and 45 min to monitor the depletion rate of ascorbic acid.

In the DTT assay, three separate aliquots of 0.45 ml of the extract were incubated at 37 °C with 90 μl of 0.1 M potassium phosphate buffer (pH 7.4) and 60 μl of 1 mM DTT. After 15, 30, and 45 min, respectively, the reactions were stopped by adding 0.5 ml of 10 % (w/v) trichloroacetic acid. The mixtures were then treated with 2 ml of Tris–EDTA solution (0.4 M Tris with 20 mM EDTA) and 50 μl of 10 mM 5,5′-dithiobis-2-nitrobenzoic acid (DTNB), and the absorbance at 412 nm was recorded.

Both methods used an initial antioxidant concentration of 100 nmol ml^{-1}. Blank filter samples were analysed using the same procedures as for the PM_{10} samples and the depletion rate was subtracted. The OP values (OP_{AA} and OPD_{TT}) were calculated based on the depletion rates of AA and DTT, respectively, and expressed per cubic meter (OP_V, nmol min^{-1} m^{-3}) and PM mass (OP_m, nmol min^{-1} μg^{-1}). OP analyses were performed in duplicate, and any sample with a coefficient of variation exceeding 10 % was reanalysed. Limits of detection were calculated as three times the standard deviation of the slope (μmol DTT min^{-1} or μmol AA min^{-1}) from blank filters. The resulting LODs were 0.22 μmol min^{-1} for the DTT assay and 0.37 μmol min^{-1} for the AA assay.

2.4. Statistical analysis

Spearman's rank correlation coefficients were calculated with SPSS software (IBM Statistics software, version 29).

3. Results

3.1. PM_{10} concentrations, chemical composition, and morphology

Indoor PM_{10} concentrations varied substantially depending on the appliance and fuel used (Table S3). Fireplace operation generated the highest PM_{10} levels indoors, averaging 319 μg m^{-3}, followed by the woodstove at 78.5 μg m^{-3} and the coal stove at 75.9 μg m^{-3}. Background PM_{10} concentrations were much lower, with levels ranging from 19.3 μg m^{-3} to 28.9 μg m^{-3}. Outdoor PM_{10} levels were generally higher than in background air but lower than indoor concentrations during combustion (Fig. S2). Organic carbon levels follow a similar pattern to PM_{10} concentrations (Table S3), with indoor environments showing the highest concentrations. Fireplace use produced the most OC indoors, averaging 128 μg m^{-3}, while woodstove and coal stove showed much lower OC levels at 15.9 and 14.3 μg m^{-3}, respectively. Background OC levels were markedly lower, ranging from 2.46 to 5.03 μg m^{-3}, while outdoor levels were slightly higher but remained below indoor concentrations (Fig. S2). The contribution of OC to PM_{10} was substantially higher during fireplace operation, averaging 40 %. This value is nearly double that observed for the woodstove (19.7 %) and coal stove (16.7 %), and clearly exceeds the outdoor OC/PM_{10}, which ranged from 10.7 % to 22.4 %. When compared to background indoor levels, measured when the appliance was not in use, the difference is even more pronounced. In this case, the OC/PM_{10} ratio averaged just 14 % for the fireplace setting, highlighting the considerable impact of active combustion on indoor PM composition. The observed WSOC concentrations also showed substantial variability across different combustion sources and environmental

settings (Fig. 1).

Indoor samples generally exhibited higher WSOC concentrations, particularly those associated with the fireplace, for which levels ranged from 14.7 to 175 μg m^{-3}. Indoor woodstove samples also showed variability, with concentrations between 0.60 and 7.49 μg m^{-3}. Coal burning produced lower indoor WSOC levels, ranging from 0.65 to 6.75 μg m^{-3}. Outdoor WSOC concentrations were generally lower than their counterparts, with concentrations ranging from 0.66 to 8.09 μg m^{-3} (Table S3, Fig. S2), reflecting variability in atmospheric conditions, emission sources and secondary formation processes (López-Caravaca et al., 2023; Snyder et al., 2009). WSOC in atmospheric aerosols originates from both primary emissions (e.g., biomass burning) and secondary formation through the oxidation of volatile organic compounds. Previous studies have shown that WSOC represents a major fraction of fine particulate organic carbon and is often strongly correlated with biomass burning tracers such as levoglucosan (Haque et al., 2021; Mayol-Bracero et al., 2002). At broader spatial scales, WSOC also reflects secondary organic aerosol (SOA) formation, with contributions that vary seasonally and geographically (López-Caravaca et al., 2023; Snyder et al., 2009).

The WSOC/OC ratio offers valuable insight into the water solubility of organic carbon and helps identify potential contributions from different sources, such as biomass burning and SOA formation (Du et al., 2014; Timonen et al., 2008; Wen et al., 2018; Zhang et al., 2022). In the present study, the WSOC/OC ratio was highly variable across different combustion sources and environment settings (Fig. 1). Indoor fireplace emissions exhibited the highest WSOC/OC ratios, reaching a maximum of 0.84, which suggests that a significant fraction of the emitted organic carbon is water-soluble. This is consistent with previous findings on biomass combustion (Kaskaoutis et al., 2022; López-Caravaca et al., 2024; Mayol-Bracero et al., 2002; Ramya et al., 2023). In contrast, indoor samples from coal burning showed much lower WSOC/OC ratios, ranging from 0.11 to 0.36, indicating that coal combustion produces a smaller fraction of WSOC compared to biomass burning. This observation aligns with previous studies reporting on emissions from residential coal combustion (Li et al., 2022). The differences in WSOC levels can be attributed to the distinct chemical compositions and combustion conditions of each fuel type. Biomass burning emissions are typically dominated by oxygen-containing organic compounds, which are more polar and water-soluble, while coal combustion emissions are enriched in sulphur- and nitrogen-containing compounds (e.g., CHOS, CHONS, CHON), many of which are less soluble and accumulate more in the water-insoluble OC fraction. Additionally, the higher nitrogen content of coal fuels correlates with a greater abundance of CHON compounds, further reducing the relative WSOC contribution. The combustion phase can also influence organic carbon composition. For example, sulphur-containing organic compounds tend to be more prominent during flaming conditions, which are common in coal burning (Zhang et al., 2024a).

Outdoor samples generally exhibited lower WSOC/OC ratios between 0.07 and 0.77, although some exceptions were noted, particularly during coal combustion (Fig. 1). Indoor background samples showed negligible WSOC and WSOC/OC values (Table S3).

The average elemental concentrations of PM_{10} varied markedly across sampling conditions and combustion sources (Fig. 2). Indoor samples from woodstove combustion exhibited the highest concentrations overall, especially for Ca (averaging 2636 ng m^{-3}), Cl, K, S and Mn. Fireplace combustion also led to elevated indoor levels of Ca, K, Cl, and S with average concentrations ranging from approximately 320 (S) to 980 ng m^{-3} (K). Inorganic emissions from wood combustion depend on the element content in the fuel, its volatility, fuel bed temperature, and the presence of binding compounds (Czech et al., 2018). Since the same fuel was used in both the woodstove and the open fireplace, the higher indoor concentrations observed during woodstove operation are mainly due to its higher combustion temperatures. In contrast, indoor samples from coal burning exhibited lower average concentrations, with each individual element generally present at levels below 350 ng m^{-3}.

Additionally, trace elements including Ti, Zn, and Sr were detected indoors, with their concentrations varying depending on the combustion appliances. The Ti concentrations measured in indoor woodstove and coal samples may be attributed to the mineral fraction of the fuels or from the entrainment of soil-derived particles adhering to the fuel prior to combustion (Vassilev et al., 2010; Xu et al., 2004). Titanium is typically regarded as a marker of crustal material and is commonly associated with soil dust (Massimi et al., 2024). Zinc concentrations were slightly higher during coal combustion, although it was also detected during wood combustion in both appliances. Commonly associated with emissions from industrial processes and traffic-related sources (Alves et al., 2022; Councell et al., 2004), Zn is also naturally present in both wood and coal (Jones et al., 2014; Xu et al., 2004). Strontium was detected at very low concentrations in all samples, with slightly higher indoor levels in both the coal- and wood-stove measurements. Despite its low abundance, this element is a relevant tracer of mineral dust, marine aerosol, and anthropogenic inputs such as biomass burning and fossil fuel combustion (Desboeufs et al., 2018).

Background levels were consistently lower than those observed

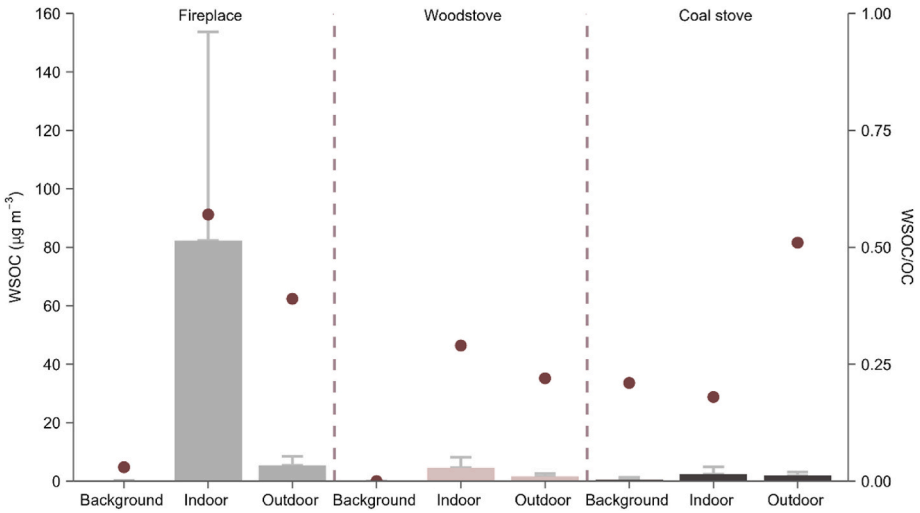

Fig. 1. Water-soluble organic carbon (WSOC) concentrations across different appliances (fireplace, woodstove, coal stove) and environments. Bars represent WSOC concentrations (mean ± standard deviation), while maroon points indicate the proportion of WSOC to OC.

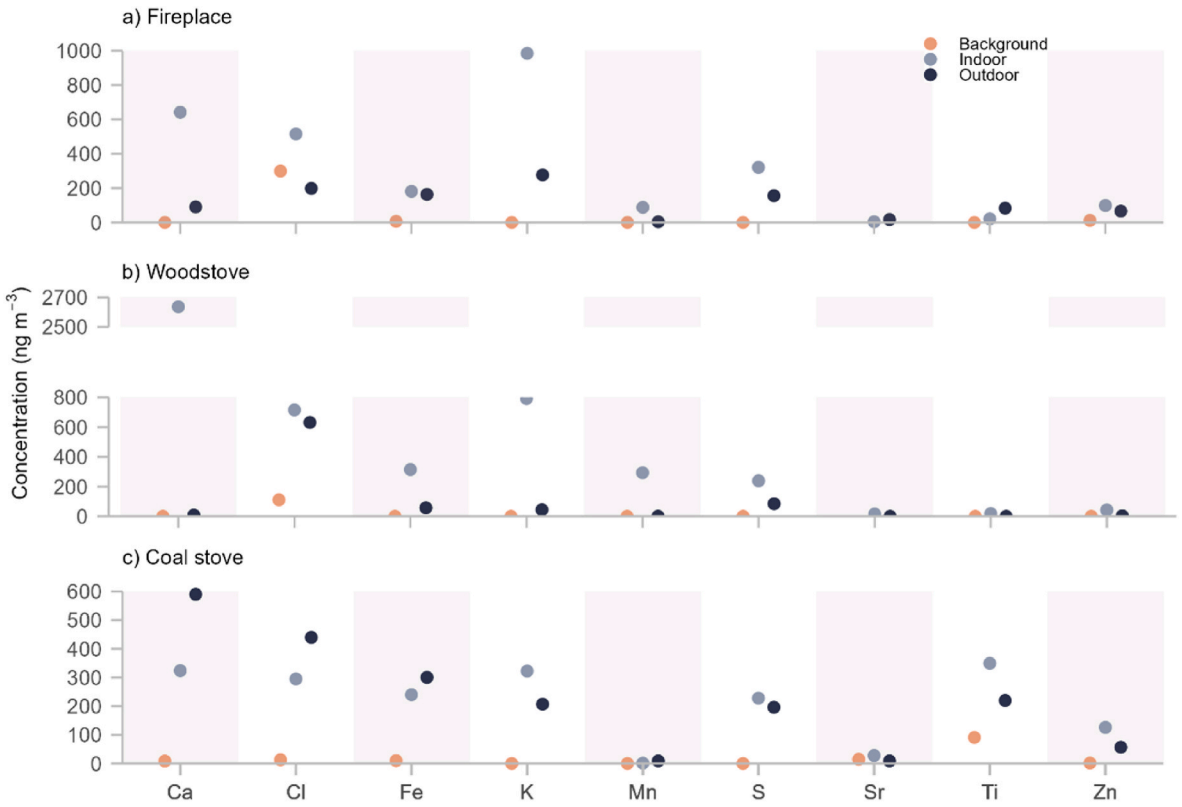

Fig. 2. Average elemental concentration of PM_{10} differentiated by type of residential heating appliances. The coloured dots denote different environmental settings.

during active wood or coal burning, often near or below 100 ng m^{-3} for most elements. These baseline values provide a useful reference, stressing the substantial increases in elemental concentrations attributable to combustion activities. During biomass combustion events, indoor concentrations were consistently higher than outdoor levels, highlighting the significant impact of residential combustion appliances on indoor air quality. In contrast, during coal combustion, higher outdoor concentrations were observed for certain elements, particularly Cl, Ca, and Fe. This pattern likely reflects the influence of local environmental conditions and outdoor sources. The sampling site, located in a rural coastal area and surrounded by forested terrain, is frequently influenced by marine aerosol and resuspended soil dust. The observed outdoor Cl enrichment is consistent with the contribution of sea-salt particles generated by wave breaking. Similarly, the elevated outdoor Ca and Fe concentrations are attributable to crustal inputs from the resuspension of local soil and dust particles (Cipoli et al., 2023).

SEM–EDS analyses of indoor samples collected during fireplace operation (Fig. 3a) revealed a consistent dominance of carbonaceous soot particles, representing 40–70 % of the analysed points. These particles showed high C content (C >50 %), frequently occurring as agglomerates with embedded silica or aluminosilicate inclusions. Such morphologies are characteristic of incomplete biomass combustion, where soot is released and subsequently coated with mineral ash phases (Andreae, 2019; Janḧall et al., 2010). The indoor confinement effect amplifies soot accumulation compared to outdoor settings, where mineral dust more strongly dilutes combustion signatures (Fleisch et al., 2020; Vicente et al., 2020; Wolf et al., 2021).

Ca- and S-rich particles were abundant in all samples, consistent with biomass ash residues. These often exhibited gypsum- or anhydrite-like compositions ($CaSO_4$ phases) or Ca-Si associations, indicating mineralisation of biomass nutrients and secondary sulphate formation during combustion and subsequent indoor accumulation (Jahn et al., 2020; Perrino et al., 2022). The recurrent presence of K and minor P further supported a biomass origin, since these are characteristic markers of wood-combustion aerosols (Andreae, 2019; Vicente and Alves, 2018). Mineral dust contributions included quartz and feldspar/clay-derived aluminosilicate particles, many of which were coated with soot. These reflected indoor resuspension of soil, construction debris, or ash residues, subsequently modified by deposition of carbonaceous matter. Such interactions between combustion emissions and background mineral dust have been reported in domestic wood-burning environments, where confined air enhances particle accumulation (Chakraborty et al., 2020; Vicente et al., 2020). Fe-rich particles were also identified, typically as Fe-bearing aluminosilicates or oxides, consistent with both wood ash transformation and soil-derived dust inputs (Adachi et al., 2022; Maschowski et al., 2019). Studies confirmed that stove type and burning conditions critically affect particle emissions (Bhattu et al., 2019; Trojanowski and Fthenakis, 2019).

Trace anthropogenic signatures were occasionally observed, including In, Ti, and Zn. In addition to the possible sources described above, these elements may derive from metallic components of appliances, building coatings, or infiltration of external particles. They have been linked to In-Ti oxide (ITO) used in electronics and architectural materials, confirming potential anthropogenic contributions to indoor aerosols (Kim et al., 2021). Barite ($BaSO_4$) was detected in one sample, likely reflecting non-combustion contamination near the sampling location (USGS, 2024). Ti-rich particles are compatible with TiO_2 paint/coating weathering (Nored et al., 2022), while In-bearing particles suggest ITO-related sources increasingly reported in ambient environments (Xu et al., 2023).

Indoor samples collected during woodstove combustion (Fig. 3b) consistently showed a dominance of carbonaceous soot and char particles. These particles were often observed as agglomerates with high carbon content (>40 wt%) and associated with oxygen, silica, and minor aluminosilicates. Similar morphologies and compositions have been reported in previous studies, in which soot has been described as forming primary carbonaceous aggregates coated with organic and inorganic ash phases (Fleisch et al., 2020; Janḧ;all et al., 2010). Soot,

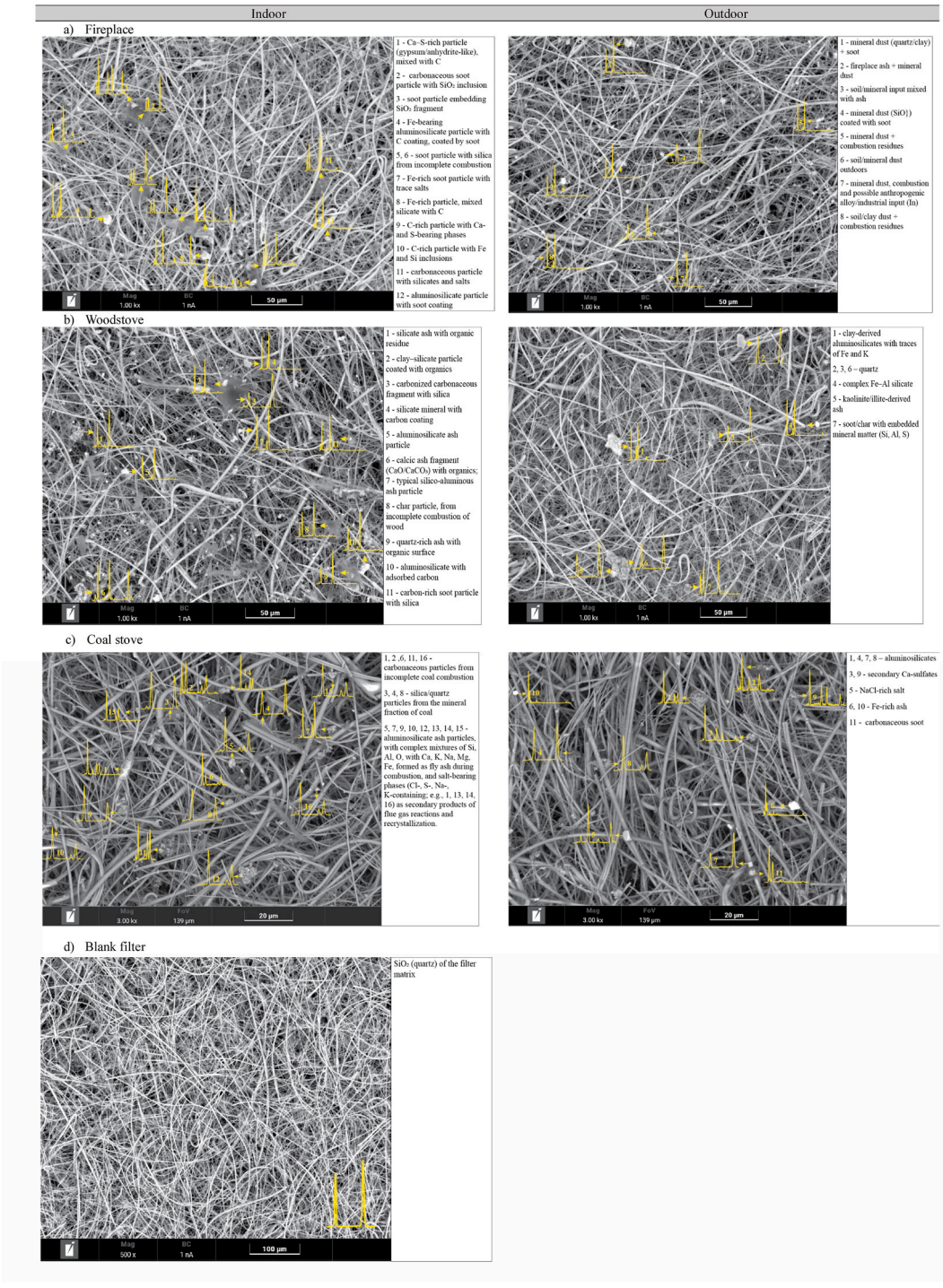

Fig. 3. SEM-EDS images for one day of experiment (indoor and outdoor sample) using the a) fireplace, b) woodstove and c) coal stove and image of (d) blank quartz filter fibres with no particles deposited, showing the spectra of the fibres (SiO_2).

ash-derived silicate particles such as aluminosilicates, quartz-rich, and Ca-bearing silicates were abundant in all samples, reflecting the mineral fraction of biomass fuel and entrained soil or dust from firewood. Ca, K, Mg, and P were frequently detected, consistent with the wood composition and their volatilisation-condensation during combustion (Vicente et al., 2020; Vicente and Alves, 2018). Calcic phases (e.g., $CaCO_3$, CaO, and Ca-silicates) were prominent in two samples, highlighting the mineralisation of Ca from biomass. The K- and P-rich ash particles identified in other samples confirmed the nutrient imprint of biomass fuel. Quartz- and feldspar-derived particles were also found, often coated with carbonaceous layers, suggesting resuspension of mineral dust from fuel or indoor environment and subsequent interaction with soot. This process of mineral-dust–soot blending has also been documented by Maschowski et al. (2019). Fe-rich particles detected in two samples consisted of Fe-oxides or Fe-bearing aluminosilicates that may derive from biomass ash transformation, soil entrainment, or possibly abrasion/corrosion of stove materials (Bhattu et al., 2019). Trace anthropogenic signatures were also found in specific cases, related to Na–Cl particles (halite-like), possibly linked to salt-treated wood or ambient deposition. In one sample, boron- and sodium-rich anomalies

could be associated with external contamination (e.g., glass or coatings).

These variations emphasise that while soot and ash are ubiquitous in these environments, the specific particle mixtures depend on combustion-related parameters and household conditions (e.g., ventilation). Stove technology and burning practices are known to substantially influence particle emissions, altering the relative abundance of soot, inorganic ash, and salts (Chakraborty et al., 2020; Trojanowski and Fthenakis, 2019). Outdoor samples collected during woodstove operation were dominated by mineral phases (quartz and aluminosilicates), with smaller contributions from soot/char and Fe-rich ash. Carbonaceous particles often contained mineral inclusions, while Fe-bearing aluminosilicates, Fe-oxides with adhered soot, and alkali aluminosilicates (feldspathic/clay-like) highlighted the coexistence of combustion residues with resuspended mineral dust. This mixed composition reflects the dilution of residential biomass combustion emissions by soil and construction dust, resulting in a higher mineral fraction outdoors than indoors, consistent with previous observations (Andreae, 2019; Janḧ;all et al., 2010; Liang et al., 2022; Vicente and Alves, 2018). Fe-rich silicate/oxide phases likely originated from biomass-ash transformations, soil inputs, or fly ash (Maschowski et al., 2019), while alkali enrichment (Na, K) in aluminosilicates reflected biomass-ash constituents incorporated into silicate matrices during combustion. Variations among samples showed shifts between mineral-dominated spectra and more ash/soot-influenced signatures, suggesting changing contributions from local sources (e.g., residential combustion), meteorology, and dust resuspension (Bhattu et al., 2019; Trojanowski and Fthenakis, 2019).

Indoor samples collected during coal combustion showed abundant fly ash particles with similar chemical composition and morphology, although particle sizes varied. Two major groups of particles were identified (Fig. 3c). The first group consisted of carbonaceous particles, characterised by high C content with associated oxygen and minor amounts of Cl, S, and Fe. These particles, including soot and char, are products of incomplete combustion and are often enriched through the adsorption of acidic gases such as HCl and SO_2. Previous studies have shown that these particles are typical of small-scale coal combustion, and are strongly associated with light absorption and negative indoor health impacts (Li et al., 2019a). The second group included mineral ash particles, mainly silica and aluminosilicates, enriched in O, Si, and Al, with variable contributions of Ca, K, Na, Fe, and Mg, representing coal mineral fraction released during combustion as fly ash. High-temperature conditions are known to induce amorphization of clay minerals, leading to the formation of aluminosilicate glassy spheres and quartz residues (Adachi et al., 2022). Trace elemental signatures provided additional insights of secondary transformations. Sulphates, e.g., $CaSO_4$ and K_2SO_4, suggested by the presence of S, Ca, and K, were consistent with secondary formation during flue gas cooling (Dang et al., 2022). Chlorides (identified Cl) likely resulted from reactions with HCl in emissions (Perrino et al., 2022). The Fe-rich aluminosilicates may contribute to enhanced reactivity and particle toxicity. The association between mineral and carbonaceous phases suggested the occurrence of heterogeneous reactions indoors. Outdoor samples contained carbonaceous material but in smaller amounts than indoor samples. They also exhibited different quantities of aluminosilicates, amorphous glass spheres, Fe oxides, calcium sulphates, and other particles composed of Al, Si, Na, K and Ca.

Generally, indoor background air samples exhibited a significantly lower number of particles compared to samples collected during combustion events, and no carbonaceous fly ash was observed.

3.2. Oxidative potential

Table 1 presents volume-normalised (OP_V) values for OP^{AA} (ascorbic acid) and OP^{DTT} (dithiothreitol) across different combustion appliances and sampling environments. Indoor OP^{AA} levels during fireplace combustion averaged 18.5 nmol min^{-1} m^{-3}, considerably higher than those measured for woodstove (4.06 nmol min^{-1} m^{-3}) and coal combustion (2.43 nmol min^{-1} m^{-3}). Background OP^{AA} values were much lower, ranging from 0.11 nmol min^{-1} m^{-3} for the woodstove to 0.55 nmol min^{-1} m^{-3} for the fireplace, on average. OP^{DTT} followed a similar pattern across indoor fuel combustion sources, with the highest values observed for the fireplace (9.06 nmol min^{-1} m^{-3}), followed by the woodstove (4.29 nmol min^{-1} m^{-3}) and coal burning (1.37 nmol min^{-1} m^{-3}). In contrast, background indoor levels were substantially lower: 0.61 nmol min^{-1} m^{-3} for the fireplace, 0.88 nmol min^{-1} m^{-3} for the woodstove, and below detection limit for the coal stove. These results reinforce the growing body of evidence demonstrating that indoor activities significantly elevate the OP of PM. Similar findings were reported by Yang et al. (2024), who examined indoor air quality in a residential home in Fairbanks, Alaska, during winter. They observed that, in the absence of occupants, indoor OP^{DTT} levels were lower than outdoor levels (I/O ratio of 0.53 ± 0.37). However, during indoor activities such as pellet stove use, cooking, and incense burning, $PM_{2.5}$ with highly variable oxidative potential was generated, with pellet stoves showing the highest and cooking the lowest OP values. The differences in OP across fuel types are also consistent with previous studies. For instance, Li et al., 2019b assessed the oxidative potential of black carbon emissions from residential coal combustion, biomass burning, and diesel exhaust in China. After isolating the BC and metal-rich fraction, they found that diesel exhaust produced the highest OP^{DTT}, followed by biomass, and finally coal combustion emissions. This trend mirrors the present study, in which biomass-related emissions (fireplace and woodstove) showed higher OP^{DTT} than coal. The higher OP associated with wood combustion PM_{10} compared with coal burning PM_{10} probably reflects differences in chemical composition. Wood burning typically releases a greater proportion of highly oxygenated and water-soluble organic compounds (e.g., quinones and compounds with hydroxyl and carbonyl groups) that efficiently generate ROS through redox cycling. Moreover, biomass burning also emits large amounts of nitrogen-containing organic compounds including nitroaromatic and nitrogen-containing bases that could increase the ROS-generation ability (Ma et al., 2018). In contrast, coal combustion emits a higher fraction of more reduced CHOS and CHNOS compounds (Zhang et al., 2024a), which tend to be less soluble and exhibit weaker redox activity. Luo et al. (2023) demonstrated that CHO- and CHNO-dominated molecular signatures, characteristic of biomass burning, enhance DTT activity, whereas sulphur-containing CHOS/CHNOS species show weaker or even inhibitory effects. These compositional differences, combined with variations in soluble metal content, provide a mechanistic basis for the higher OP associated with wood-derived PM relative to coal-derived PM.

In the present study, indoor OP_V values for the fireplace were markedly higher than their corresponding outdoor levels, with average OP^{AA} and OP^{DTT} approximately ten to four times greater indoors,

Table 1
Average, minimum, and maximum OP_V (nmol min^{-1} m^{-3}) levels in different environments.

		OP^{AA}		OP^{DTT}	
Appliance	Environment	Average	min - max	Average	min - max
Fireplace	Indoor (N = 4)	18.5	3.83–27.6	9.06	3.57–17.4
	Background (N = 4)	0.55	bdl - 1.33	0.61	0.072–1.83
	Outdoor (N = 4)	1.91	1.28–2.26	2.06	0.97–2.83
Woodstove	Indoor (N = 3)	4.06	1.56–7.35	4.29	3.13–6.03
	Background (N = 2)	0.11	bdl - 0.22	0.88	bdl - 1.75
	Outdoor (N = 3)	1.23	1.13–1.31	1.83	1.53–2.00
Coal stove	Indoor (N = 5)	2.43	1.56–4.03	1.37	bdl - 3.35
	Background (N = 2)	0.50	0.41–0.58	bdl	–
	Outdoor (N = 5)	2.14	1.74–2.03	1.01	bdl - 2.00

respectively. The indoor-outdoor difference was smaller for the woodstove (2 to 3-fold higher) while for the coal stove, indoor OP values (AA and DTT) were comparable to those measured outdoors (Table 1).

The outdoor OP values observed in the present study fall within the range reported by Massimi et al. (2024) for the Sacco River Valley in Italy, where OP^{DTT} varied from 0.27 to 3.9 nmol min^{-1} m^{-3} and OP^{AA} from 0.035 to 9.3 nmol min^{-1} m^{-3}. Their 18-month monitoring campaign, conducted between October 2020 and May 2022, identified biomass burning as the primary source of OP^{DTT}, while non-exhaust traffic emissions (e.g., brake and tyre wear) were found to significantly contribute to OP^{AA} levels. Similarly, Molina et al. (2023), conducted a full-year assessment of aerosol OP across multiple PM fractions in two Chilean cities. They reported average volume-normalised OP^{DTT} values ranging from 0.15 to 1.52 nmol min^{-1} m^{-3} for PM_{10} in Santiago and from 0.09 to 1.31 nmol min^{-1} m^{-3} in Chillán, with considerably higher values observed during winter due to intense biomass-burning emissions in southern Chile. OP was markedly higher during cold months in regions dominated by residential wood combustion, whereas in Santiago summer maxima were linked to enhanced SOA formation driven by photochemistry. On the other hand, the results of this study contrast with those of Pietrogrande et al. (2021), who carried out a sampling campaign at an Alpine rural site during winter 2016–2017 to assess the contribution of wood burning emissions to the OP of PM_{10}. The mean OP values at this rural location were lower than those obtained in the outdoor environments of present study, with OP^{DTT} averaging 0.33 ± 0.07 nmol min^{-1} m^{-3} and OP^{AA} at 0.28 ± 0.08 nmol min^{-1} m^{-3}. Additional insight is provided by the large-scale synthesis of OP conducted by Weber et al. (2021), who analysed more than 1700 PM_{10} samples across 14 French locations using DTT and AA assays. Their results demonstrate that OP^{DTT} is strongly driven by primary road traffic emissions, which exhibited the highest intrinsic OP among all identified sources, surpassing even biomass burning. On the contrary, OP^{AA} was influenced almost exclusively by biomass burning and road traffic, with other sources such as nitrate-rich aerosols and aged sea salt showing negligible redox activity. Weber et al. (2021) also documented clear seasonal patterns, with OP values peaking in winter at Alpine valley sites due to thermal inversions and enhanced accumulation of wood-burning emissions, while traffic-related OP contributions remained more consistent throughout the year.

It should be noted, however, that direct comparisons between studies must be interpreted with caution, as differences in oxidative potential values may arise from the diversity of analytical protocols applied. Indeed, efforts are currently underway to harmonise OP measurement methodologies and improve cross-study comparability (Dominutti et al., 2024). In addition to the variability introduced by the different analytical protocols used to determine OP, differences in sampling strategy, such as the sampling period, duration, and number of collected samples, can also substantially influence the obtained results. Furthermore, environmental and source-related factors that affect PM levels and composition may consequently influence the measured OP.

The intrinsic oxidative potential (OP_m, nmol min^{-1} μg^{-1}) showed distinct patterns depending on the appliance type and sampling environment (Table S4). The highest OP^{AA} values were recorded for the fireplace (0.057 nmol min^{-1} μg^{-1}), followed by woodstove (0.052 nmol min^{-1} μg^{-1}) and coal stove (0.044 nmol min^{-1} μg^{-1}). In contrast, OP^{DTT} values were higher for the woodstove (0.055 nmol min^{-1} μg^{-1}), on average, more than twice those of the fireplace (0.027 nmol min^{-1} μg^{-1}) and coal stove (0.021 nmol min^{-1} μg^{-1}). OP^{AA} values during fireplace operation were considerably higher than both background (0.023 nmol min^{-1} μg^{-1}) and outdoor (0.024 nmol min^{-1} μg^{-1}) environments. In contrast, OP^{DTT} values were relatively similar across environments (0.024–0.027 nmol min^{-1} μg^{-1}). For woodstove, both OP^{AA} and OP^{DTT} were clearly elevated in indoor and outdoor samples compared with background levels. Outdoor samples displayed the highest OP^{DTT} values (0.065 nmol min^{-1} μg^{-1}) and relatively high OP^{AA} (0.045 nmol min^{-1} μg^{-1}). In the case of coal stove, the outdoor environment showed the highest OP^{AA} values overall (average 0.065, up to 0.11 nmol min^{-1} μg^{-1}). The OP^{DTT} values were generally lower and more variable.

The findings of the present study align closely with previous research on the OP of emissions from solid-fuel combustion. Isenor et al. (2024) reported that for wood fuels, mass-normalised DTT activity (OP_m) was sometimes higher in improved or forced-draft cookstoves than in traditional stoves (three-stone fire cookstove); however, OP_V, a more relevant proxy for exposure, was substantially lower due to the markedly reduced PM emissions. The authors also compared wood and charcoal and showed that wood fuels produced higher OP_V than charcoal. Regarding the fuel, Zhang et al. (2024b) compared emissions from raw biomass, coal, and biomass pellets burned in both traditional and improved stoves using the DTT assay. They reported that pellet emissions exhibited lower OP_m than raw biomass; however, no statistically significant differences were observed between the OP_m of coal smoke and pellet fuel. Although studies quantifying OP from PM exposure in real-world solid-fuel settings remain limited, some comparisons can be drawn. Sharma et al. (2024) conducted size-resolved DTT assays in rural kitchens in northeastern India and reported that OP_V in firewood and mixed-biomass kitchens was enhanced by a factor of 5 relative to LPG-using homes. In contrast, OP_m was similar between LPG and firewood kitchens, with mixed-biomass fuels exhibiting the highest intrinsic particle toxicity. Their size-distribution analysis further showed that biomass-burning emissions produced trimodal OP_V profiles, with strong contributions from both ultrafine and coarse particles. Contrasting results were reported by Brehmer et al. (2019). The authors evaluated the OP of personal and household $PM_{2.5}$ in a rural region of southwestern China where biomass is widely used for cooking and heating. Using the DTT assay, the authors reported moderate and spatially variable OP_m values, with no clear enhancement in homes relying on solid fuels compared with those using cleaner fuels. Their correlation analysis showed that DTT activity was driven primarily by transition metals such as Cu, Mn, and Zn, rather than by biomass-burning tracers. A key methodological difference relative to the present study is that Brehmer et al. (2019) analysed unfiltered PM extracts, thereby including both soluble and insoluble particle fractions in the DTT assay.

Spearman correlation coefficients between OP^{DTT}, OP^{AA} and PM_{10} are reported in Fig. 4. OP^{DTT} and OP^{AA} exhibited a significant correlation ($r = 0.587$, $p < 0.05$) indoors, whereas no significant correlation was found outdoors ($r = 0.179$, $p > 0.05$). These findings are in line with previous studies reporting significant correlations between these two assays for ambient PM across diverse environments (Calas et al., 2019; Clemente et al., 2023; Gómez-Sánchez et al., 2024; Pietrogrande et al., 2021). Regarding the correlation between OP and PM_{10} concentrations, no significant associations were observed in outdoor samples ($p > 0.05$), whereas both assays showed significant correlations with PM_{10} indoors ($p < 0.05$). The absence of significant correlations outdoors suggests that particle toxicity may be more strongly influenced by chemical composition than by mass concentration alone (Yang et al., 2024). On the other hand, the significant correlations observed indoors may reflect the influence of dominant indoor sources contributing simultaneously to PM mass and oxidative potential. In the literature, contrasting results have been reported (Calas et al., 2019; Fang et al., 2016; Kurihara et al., 2022). For instance, Fang et al. (2016) examined the OP of PM samples collected across multiple seasons and contrasting environments in the southeastern United States. Sampling was conducted at seven outdoor sites, including urban, near-road (two sites adjacent to interstate highways), and rural locations. They found that AA activity was elevated at roadside and traffic-impacted sites but did not correlate with PM mass overall, whereas DTT activity showed a strong and consistent association with PM mass across the different sites and temporal gradients. In contrast, Calas et al. (2019) studied the OP of PM_{10} in seven urban background environments across France during different seasons. Their findings showed that both AA and DTT assays were consistently and significantly correlated with PM_{10}, although the strength of the correlation varied by season and city.

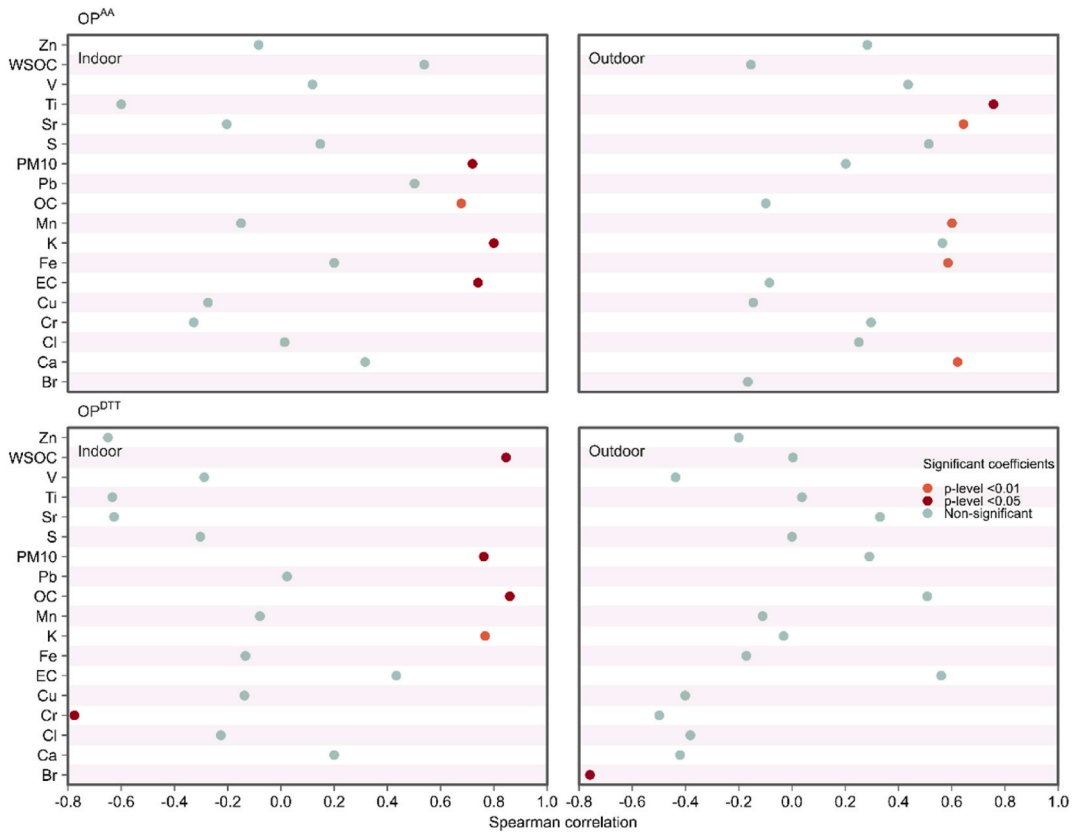

Fig. 4. Spearman correlation coefficients between PM-bound constituents (μg m^{-3}) and oxidative potential (nmol min^{-1} m^{-3}) by environment (N = 12 indoor and N = 12 outdoor). The upper panel displays the correlations using the AA method. The lower panel shows the corresponding correlations obtained with the DTT method, based on the same environments and sampling periods as in the AA analysis.

Indoors, both OP^{AA} and OP^{DTT} showed significant correlations with OC ($r = 0.678$ and $r = 0.860$, $p < 0.05$ and < 0.01, respectively). Significant correlations with WSOC ($r = 0.846$, $p < 0.01$) were observed only for OP^{DTT}, whereas EC was correlated with OP^{AA} ($r = 0.741$, $p < 0.01$). These associations support the contribution of carbonaceous fractions, particularly water-soluble organics, to oxidative potential (Bates et al., 2019; Gómez-Sánchez et al., 2024; Janssen et al., 2014; Li et al., 2025; Sharma et al., 2024; Wang et al., 2018; Zhang et al., 2024b). Previous studies have shown that the OP^{AA} assay is generally less sensitive to organic fractions than OP^{DTT} (Bates et al., 2019; Famiyeh et al., 2023; Fang et al., 2016; Molina et al., 2020; Rao et al., 2020). Thus, the observed OP^{AA} correlations with OC may result from co-emission of these species with redox-active elements. Sharma et al. (2024) explored size-resolved OP in Indian rural kitchens and found that, in firewood-using kitchens, WSOC and barium together accounted for nearly half the OP^{DTT} variability. In the present study, both OP assays were significantly correlated with potassium (OP^{AA}: $r = 0.800$, $p < 0.01$ and OP^{DTT}: $r = 0.717$, $p < 0.05$), indicating a potential contribution of biomass combustion to indoor particle toxicity. Similarly, Pietrogrande et al. (2021) investigated PM_{10} in a rural Alpine area, where wood burning is prevalent during winter, and found that both DTT and AA assays were strongly associated with biomass burning markers, including WSOC, polycyclic aromatic hydrocarbons, anhydrosugars, and soluble potassium. In a source apportionment study conducted by Fang et al. (2016) in the southeastern United States, biomass burning was identified as a major contributor to DTT activity, but not to AA activity. No other significant correlations were identified indoors.

Outdoors, only weak to moderate correlations were found between OP and OC, and none reached statistical significance. OP^{AA} showed a significant positive correlation with calcium ($r = 0.623$, $p < 0.05$), titanium ($r = 0.758$, $p < 0.01$), iron ($r = 0.587$, $p < 0.05$) and with strontium ($r = 0.645$, $p < 0.05$), indicating a likely influence from crustal or abrasion-derived particles. This is in agreement with previous studies highlighting that AA is more sensitive to PM components generated by mechanical or abrasion processes, which are more abundant in the coarse fraction (Massimi et al., 2020; Molina et al., 2020; Rao et al., 2020). Additionally, significant correlations were detected between OP^{AA} and manganese ($r = 0.602$, $p < 0.05$). Mn is redox-active, meaning it can cycle between oxidation states ($Mn^{2+}/Mn^{3+}/Mn^{4+}$) and catalyse the formation of ROS (Martinez-Finley et al., 2013). For OP^{DTT}, on the other hand, no significant positive correlations were detected.

These findings highlight the distinct chemical drivers of OP in indoor and outdoor air. The lack of significant correlations with commonly redox-active elements, specially indoors, may be explained by their low concentrations, insoluble forms, or competitive interactions in complex atmospheric matrices (Shahpoury et al., 2021; Yu et al., 2024, 2021). Additionally, the relatively limited number of samples analysed in this study may have reduced the statistical power to detect significant associations.

3.3. Limitations

While this study provides valuable insights into the composition, morphology, and OP of indoor PM_{10} from residential solid fuel combustion, some limitations should be acknowledged. The overall number of samples collected was relatively small, which may affect the robustness and representativeness of the results. A limited sample size reduces the stability of average values and the statistical power of correlation analyses between PM-bound constituent's concentrations and OP. Furthermore, due to the small number of replicates, no statistical analyses were performed to test for significant differences between

combustion appliances and environments, which could have provided additional depth to the interpretation of the results.

Another important limitation concerns the experimental conditions, which were conducted under minimal ventilation (with doors and windows closed). Although this setup may resemble certain real-world conditions, it does not capture the full range of air exchange scenarios typical of occupied dwellings, such as the presence of open windows or the use of extractor fans. Ventilation strongly influences indoor PM_{10} dynamics by affecting pollutant dilution, removal rates, and mixing with outdoor air. The absence of experiments under different ventilation scenarios therefore limits the extrapolation of these findings to diverse household conditions. Future studies should incorporate controlled ventilation scenarios to better quantify how air exchange rates modulate indoor PM levels, chemical composition, and toxicity.

Additionally, despite the application of a consistent operating protocol (e.g., ignition procedure, batch number, and fuel mass), day-to-day variations in indoor PM concentrations, PM composition and OP were observed. These fluctuations are probably driven by subtle differences in stove operation, combustion dynamics, and meteorological conditions influencing the chimney's natural draught. Variations in draught, governed by factors such as flue-gas temperature, chimney height, and ambient air conditions, affect the air-to-fuel ratio and combustion temperature, thereby altering pollutant formation and emissions (Drozdzol et al., 2023; Endriss et al., 2021; Kausley and Pandit, 2010).

Although the contribution of secondary organic aerosols to indoor PM_{10} was not quantified in the present study, SOA can constitute a substantial fraction of indoor organic aerosol under certain conditions (Waring, 2014) and has been shown to exhibit notable oxidative potential (Jiang et al., 2016; Utinger et al., 2025). Given the short duration of the indoor combustion events examined in this study and the expectedly low oxidant levels and photochemical activity, substantial SOA formation is unlikely. Nevertheless, future work could evaluate potential SOA contributions to indoor PM composition and OP to refine the overall toxicity assessment.

4. Conclusions

This study investigated the chemical composition, morphology and oxidative potential of particulate matter (PM_{10}) collected during the operation of common fuel-burning appliances (fireplace, woodstove, and coal stove) in indoor environments, outdoors and in the absence of the indoor source (background). Indoor air quality was affected by the type of fuel and combustion appliance used. Among the tested devices, the fireplace generated the highest indoor PM_{10}, OC, and WSOC concentrations, followed by the woodstove and the coal stove. These values were substantially higher than background levels, highlighting the impact of combustion sources on indoor air quality. WSOC/OC ratios were also highest for fireplace emissions, reaching up to 0.84, indicating a predominance of water-soluble organics typically associated with biomass burning. In contrast, coal combustion yielded much lower ratios (0.11–0.36), consistent with less soluble sulphur- and nitrogen-based compounds. Woodstove combustion contributed the highest indoor levels of elements such as calcium, chlorine, potassium, and sulphur, whereas coal combustion resulted in the lowest elemental concentrations. Outdoor samples displayed lower concentrations during indoor biomass combustion for most of the measured components, whereas higher levels of chlorine, calcium, and iron were observed outside during coal combustion. Morphological analysis revealed that fuel type strongly controls particle shape, composition, and inclusions, with biomass producing soot-rich emissions and coal producing abundant spherical fly ash and salts. Indoors enhanced soot accumulation was observed, while outdoor air showed less prevalence of soot particles and greater mixing with mineral dust. Background samples showed minimal particulate presence. The presence of soot-coated mineral grains, mixed aluminosilicate–carbonaceous aggregates, and sulphate-rich surface layers indicates that particle mixing and ageing processes occur indoors. These transformations likely contribute to the observed OP responses.

Oxidative potential (OP_V), evaluated by the OP^{AA} and OP^{DTT} assays, was highest during fireplace use, indicating a greater oxidative burden. Indoors, both assays correlated strongly with PM_{10}, OC and potassium. In outdoor air, the correlations were weaker and mostly non-significant for OP^{DTT}, suggesting that either the lower concentrations or the specific chemical forms of redox-active species may limit their contribution to the overall oxidative potential. In contrast, OP^{AA} exhibited significant correlations with several PM-bound elements (e.g., calcium, titanium, iron, strontium, and manganese). The OP_m results from the DTT assay indicate that, on a per-mass basis, particles emitted during woodstove operation exhibited higher oxidative activity, and thus greater intrinsic toxicity, than those produced by the other combustion appliances.

It is important to clarify that the lower indoor PM_{10} concentrations and OP measured during coal combustion, compared with wood combustion, particularly in fireplaces, should not be interpreted as evidence that coal burning is a safer household heating practice. The apparent differences observed in the present study reflect the specific appliance design, combustion efficiency, and fuel characteristics under the controlled conditions of this study. Coal remains a major source of air pollutants such as sulphur oxides, polycyclic aromatic hydrocarbons, and trace metals (e.g., arsenic), not evaluated in the present work. Therefore, the present results should be viewed as a comparative assessment of indoor emission dynamics under distinct combustion scenarios, not as a recommendation for fuel substitution. From a public health perspective, reducing or eliminating the use of all solid fuels indoors remains the most effective strategy for improving indoor air quality and reducing exposure.

CRediT authorship contribution statement

Estela D. Vicente: Writing – original draft, Visualization, Methodology, Investigation, Formal analysis, Conceptualization. **Isabella Charres:** Writing – review & editing, Visualization, Methodology, Investigation. **Yago Cipoli:** Writing – review & editing, Validation, Methodology, Investigation. **Ana I. Calvo:** Writing – review & editing, Resources, Project administration, Funding acquisition. **Roberto Fraile:** Writing – review & editing, Resources, Funding acquisition. **Carla Candeias:** Writing – review & editing, Visualization, Resources, Methodology, Investigation, Formal analysis. **Fernando Rocha:** Writing – review & editing, Resources. **Nuria Galindo:** Writing – review & editing, Supervision, Resources, Project administration, Funding acquisition. **Eduardo Yubero:** Writing – review & editing, Resources, Funding acquisition. **Célia Alves:** Writing – review & editing, Resources, Project administration, Funding acquisition.

Declaration of competing interest

The authors declare that they have no known competing financial interests or personal relationships that could have appeared to influence the work reported in this paper.

Acknowledgments

Estela Vicente acknowledges the research contract under Scientific Employment Stimulus (DOI:10.54499/2022.00399.CEECIND/CP1720/CT0012) from the FCT - Fundação para a Ciência e a Tecnologia I.P. FCT is also acknowledged for the PhD scholarships to Y. Cipoli (SFRH/BD/04992/2021) and I. Charres (DOI:10.54499/2022.12142.BD). This work was supported by national funds through FCT, under the project/grant UID/50006 + LA/P/0094/2020 (doi.org/10.54499/LA/P/0094/2020) and through the project "Air Pollution in an African Megacity: Source Apportionment and Health Implications" (APAM, DOI: 10.54499/2022.04240.PTDC). Oxidative potential assays and the chemical characterisation of PM_{10} samples were partially funded by MCIN/AEI/10.13039/501100011033 and the "European Union

NextGenerationEU/PRTR" (CAMBIO project, ref. TED2021-131336B-I00) and by MICIU/AEI/10.13039/501100011033 and ERDF/EU (TOXICAR project, ref. PID2023-149608OB-I00) and the sampling by MICIU/AEI/10.13039/501100011033 and by FEDER, EU (PID2023-152799OB-I00 project).

Appendix A. Supplementary data

Supplementary data to this article can be found online at https://doi.org/10.1016/j.envpol.2025.127510.

Data availability

Data will be made available on request.

References

Adachi, K., Dibb, J.E., Scheuer, E., Katich, J.M., Schwarz, J.P., Perring, A.E., Mediavilla, B., Guo, H., Campuzano-Jost, P., Jimenez, J.L., Crawford, J., Soja, A.J., Oshima, N., Kajino, M., Kinase, T., Kleinman, L., Sedlacek, A.J., Yokelson, R.J., Buseck, P.R., 2022. Fine ash-bearing particles as a major aerosol component in biomass burning smoke. J. Geophys. Res. Atmos. 127, 1–22. https://doi.org/10.1029/2021JD035657.

Alves, C., Evtyugina, M., Vicente, E., Vicente, A., Rienda, I.C., de la Campa, A.S., Tomé, M., Duarte, I., 2022. $PM_{2.5}$ chemical composition and health risks by inhalation near a chemical complex. J. For. Environ. 124, 860–874. https://doi.org/10.1016/J.JES.2022.02.013. Sci.

Andreae, M., 2019. Emission of trace gases and aerosols from biomass burning. Global biogeochemical. At. Chem. Phys. 15 (4), 955–966. https://doi.org/10.1029/2000GB001382.

Bates, J.T., Fang, T., Verma, V., Zeng, L., Weber, R.J., Tolbert, P.E., Abrams, J.Y., Sarnat, S.E., Klein, M., Mulholland, J.A., Russell, A.G., 2019. Review of acellular assays of ambient particulate matter oxidative potential: methods and relationships with composition, sources, and health effects. Environ. Sci. Technol. 53, 4003–4019. https://doi.org/10.1021/acs.est.8b03430.

Bhattu, D., Zotter, P., Zhou, J., Stefenelli, G., Klein, F., Bertrand, A., Temime-Roussel, B., Marchand, N., Slowik, J.G., Baltensperger, U., Prevot, A.S.H., Nussbaumer, T., Haddad, I. El, Dommen, J., 2019. Effect of stove technology and combustion conditions on gas and particulate emissions from residential biomass combustion. Environ. Sci. Technol. 53, 2209–2219. https://doi.org/10.1021/acs.est.8b05020.

Brehmer, C., Lai, A., Clark, S., Shan, M., Ni, K., Ezzati, M., Yang, X., Baumgartner, J., Schauer, J.J., Carter, E., 2019. The oxidative potential of personal and household $PM_{2.5}$ in a rural setting in Southwestern China. Environ. Sci. Technol. 53, 2788–2798. https://doi.org/10.1021/acs.est.8b05120.

Calas, A., Uzu, G., Besombes, J.L., Martins, J.M.F., Redaelli, M., Weber, S., Charron, A., Albinet, A., Chevrier, F., Brulfert, G., Mesbah, B., Favez, O., Jaffrezo, J.L., 2019. Seasonal variations and chemical predictors of oxidative potential (OP) of particulate matter (PM), for seven urban French sites. Atmosphere 10, 1–20. https://doi.org/10.3390/atmos10110698.

Cao, T., Li, M., Zou, C., Fan, X., Song, J., Jia, W., Yu, C., Yu, Z., Peng, P., 2021. Chemical composition, optical properties, and oxidative potential of water-and methanol-soluble organic compounds emitted from the combustion of biomass materials and coal. Atmos. Chem. Phys. 21, 13187–13205. https://doi.org/10.5194/acp-21-13187-2021.

Chakraborty, R., Heydon, J., Mayfield, M., Mihaylova, L., 2020. Indoor air pollution from residential stoves: examining the flooding of particulate matter into homes during real-world use. Atmosphere 11. https://doi.org/10.3390/atmos11121326.

Chiari, M., Yubero, E., Calzolai, G., Lucarelli, F., Crespo, J., Galindo, N., Nicolás, J.F., Giannoni, M., Nava, S., 2018. Comparison of PIXE and XRF analysis of airborne particulate matter samples collected on Teflon and quartz fibre filters. Nucl. Instrum. Methods Phys. Res. Sect. B Beam Interact. Mater. Atoms 417, 128–132. https://doi.org/10.1016/j.nimb.2017.07.031.

Cipoli, Y.A., Alves, C., Rapuano, M., Evtyugina, M., Rienda, I.C., Kováts, N., Vicente, A., Giardi, F., Furst, L., Nunes, T., Feliciano, M., 2023. Nighttime–daytime PM_{10} source apportionment and toxicity in a remoteness inland city of the Iberian Peninsula. Atmos. Environ. 303. https://doi.org/10.1016/j.atmosenv.2023.119771.

Clemente, Gil-Moltó, J., Yubero, E., Juárez, N., Nicolás, J.F., Crespo, J., Galindo, N., 2023. Sensitivity of PM_{10} oxidative potential to aerosol chemical composition at a Mediterranean urban site: ascorbic acid versus dithiothreitol measurements. Air Qual. Atmos. Health 16, 1165–1172. https://doi.org/10.1007/s11869-023-01332-1.

Councell, T.B., Duckenfield, K.U., Landa, E.R., Callender, E., 2004. Tire-wear particles as a source of zinc to the environment. Environ. Sci. Technol. 38, 4206–4214. https://doi.org/10.1021/es034631f.

Czech, H., Miersch, T., Orasche, J., Abbaszade, G., Sippula, O., Tissari, J., Michalke, B., Schnelle-Kreis, J., Streibel, T., Jokiniemi, J., Zimmermann, R., 2018. Chemical composition and speciation of particulate organic matter from modern residential small-scale wood combustion appliances. Sci. Total Environ. 612, 636–648. https://doi.org/10.1016/j.scitotenv.2017.08.263.

Dang, C., Segal-Rozenhaimer, M., Che, H., Zhang, L., Formenti, P., Taylor, J., Dobracki, A., Purdue, S., Wong, P.S., Nenes, A., Sedlacek, A., Coe, H., Redemann, J., Zuidema, P., Howell, S., Haywood, J., 2022. Biomass burning and marine aerosol processing over the southeast Atlantic Ocean: a TEM single-particle analysis. Atmos. Chem. Phys. 22, 9389–9412. https://doi.org/10.5194/acp-22-9389-2022.

Desboeufs, K., Nguyen, E.B., Chevaillier, S., Triquet, S., Dulac, F., Atmopshériques, S., Cnrs, U.M.R., Créteil, U.P., 2018. Fluxes and sources of nutrient and trace metal atmospheric deposition in the northwestern Mediterranean. Atmos. Chem. Phys. 18, 14477–14492. https://doi.org/10.5194/acp-18-14477-2018.

Dominutti, P.A., Jaffrezo, J., Marsal, A., Mhadhbi, T., Elazzouzi, R., Rak, C., Cavalli, F., Putaud, J.-P., Bougiatioti, A., Mihalopoulos, N., Paraskevopoulou, D., Mudway, I., Nenes, A., Daellenbach, K.R., Banach, C., Campbell, S.J., Cigánková, H., Contini, D., Evans, G., Georgopoulou, M., Ghanem, M., Glencross, D.A., Guascito, M.R., Herrmann, H., Iram, S., Jovanovi, M., Jovaševic-Stojanovic, M., Kalberer, M., Kooter, I.M., Paulson, S.E., Patel, A., Perdrix, E., Pietrogrande, M.C., Mikuška, P., Sauvain, J.-J., Seitanidi, K., Shahpoury, P., Souza, E.J.d.S., Steimer, S., Stevanovic, S., Suarez, G., Subramanian, P.S.G., Utinger, B., Os, M.F. van, Verma, V., Wang, X., Weber, R.J., Yang, Y., Querol, X., Hoek, G., Harrison, R.M., Uzu, G., 2024. An interlaboratory comparison to quantify oxidative potential measurement in aerosol particles: challenges and recommendations for harmonisation. Atmos. Meas. Tech. 18, 177–195. https://doi.org/10.5194/amt-18-177-2025.

Drozdzol, K., Junga, R., Beben, D., Kielland, T., Jarzynski, P., 2023. The influence of the fan-controlled chimney draft on the pollutants emission to the environment. In: Semião, J.F.L.C., Sousa, N.M.S., da Cruz, R.M.S., Prates, G.N.D. (Eds.), Increase 2023. Advances in Sustainability Science and Technology. Springer, Cham, pp. 141–156. https://doi.org/10.1007/978-3-031-44006-9_11.

Du, Z., He, K., Cheng, Y., Duan, F., Ma, Y., Liu, J., Zhang, X., Zheng, M., Weber, R., 2014. A yearlong study of water-soluble organic carbon in Beijing I: sources and its primary vs. secondary nature. Atmos. Environ. 92, 514–521. https://doi.org/10.1016/j.atmosenv.2014.04.060.

Endriss, F., Grammer, P., Russ, M., Thorwarth, H., 2021. Impact of chimney-draught conditions on combustion and emission behavior of a wood-burning stove. Chem.-Ing.-Tech. 93, 412–420. https://doi.org/10.1002/cite.202000098.

Famiyeh, Lord, Jia, C., Chen, K., Tang, Y.T., Ji, D., He, J., Guo, Q., 2023. Size distribution and lung-deposition of ambient particulate matter oxidative potential: a contrast between dithiothreitol and ascorbic acid assays. Environ. Pollut. 336, 122437. https://doi.org/10.1016/j.envpol.2023.122437.

Fang, T., Verma, V., T Bates, J., Abrams, J., Klein, M., Strickland, J.M., Sarnat, E.S., Chang, H.H., Mulholland, A.J., Tolbert, E.P., Russell, G.A., Weber, J.R., 2016. Oxidative potential of ambient water-soluble $PM_{2.5}$ in the southeastern United States: contrasts in sources and health associations between ascorbic acid (AA) and dithiothreitol (DTT) assays. Atmos. Chem. Phys. 16, 3865–3879. https://doi.org/10.5194/acp-16-3865-2016.

Fleisch, A.F., Rokoff, L.B., Garshick, E., Grady, S.T., Chipman, J.W., Baker, E.R., Koutrakis, P., Karagas, M.R., 2020. Residential wood stove use and indoor exposure to $PM_{2.5}$ and its components in Northern New England. J. Expo. Sci. Environ. Epidemiol. 30, 350–361. https://doi.org/10.1038/s41370-019-0151-4.

Gao, D., Ripley, S., Weichenthal, S., Godri Pollitt, K.J., 2020. Ambient particulate matter oxidative potential: chemical determinants, associated health effects, and strategies for risk management. Free Radic. Biol. Med. 151, 7–25. https://doi.org/10.1016/j.freeradbiomed.2020.04.028.

Gómez-Sánchez, N., Galindo, N., Alfosea-Simón, M., Nicolás, J.F., Crespo, J., Yubero, E., 2024. Chemical composition of PM_{10} at a rural site in the western Mediterranean and its relationship with the oxidative potential. Chemosphere 363, 142880. https://doi.org/10.1016/j.chemosphere.2024.142880.

Gurjar, B.R., Molina, L.T., Ojha, C.S. (Eds.), 2010. Air Pollution. Health and Environmental Impacts. CRC Press, Taylor & Francis Group, New York.

Haque, M.M., Kawamura, K., Deshmukh, D.K., Kunwar, B., Kim, Y., 2021. Biomass burning is an important source of organic aerosols in interior Alaska. J. Geophys. Res. Atmos. 126, 1–21. https://doi.org/10.1029/2021JD034586.

He, L., Zhang, J., 2023. Particulate matter (PM) oxidative potential: measurement methods and links to PM physicochemical characteristics and health effects. Crit. Rev. Environ. Sci. Technol. 53, 177–197. https://doi.org/10.1080/10643389.2022.2050148.

Isenor, B.H., Downey, J.P., Whidden, S.A., Fitzgerald, M.M., Wong, J.P.S., 2024. Oxidative potential of fine particulate matter emitted from traditional and improved biomass cookstoves. Environ. Sci.: Atmos. 4, 202–213. https://doi.org/10.1039/d3ea00135k.

Jahn, L.G., Polen, M.J., Jahl, L.G., Brubaker, T.A., Somers, J., Sullivan, R.C., 2020. Biomass combustion produces ice-active minerals in biomass-burning aerosol and bottom ash. Proc. Natl. Acad. Sci. U. S. A 117, 21928–21937. https://doi.org/10.1073/pnas.1922128117.

Janhall, S., Andreae, M.O., Pöschl, U., 2010. Biomass burning aerosol emissions from vegetation fires: particle number and mass emission factors and size distributions. Atmos. Chem. Phys. 10, 1427–1439. https://doi.org/10.5194/acp-10-1427-2010.

Janssen, N.A.H., Yang, A., Strak, M., Steenhof, M., Hellack, B., Gerlofs-Nijland, M.E., Kuhlbusch, T., Kelly, F., Harrison, R., Brunekreef, B., Hoek, G., Cassee, F., 2014. Oxidative potential of particulate matter collected at sites with different source characteristics. Sci. Total Environ. 472, 572–581. https://doi.org/10.1016/j.scitotenv.2013.11.099.

Jiang, H., Jang, M., Sabo-Attwood, T., Robinson, S.E., 2016. Oxidative potential of secondary organic aerosols produced from photooxidation of different hydrocarbons using outdoor chamber under ambient sunlight. Atmos. Environ. 131, 382–389. https://doi.org/10.1016/j.atmosenv.2016.02.016.

Jiang, K., Xing, R., Luo, Z., Huang, W., Yi, F., Men, Y., Zhao, N., Chang, Z., Zhao, J., Pan, B., Shen, G., 2024. Pollutant emissions from biomass burning: a review on emission characteristics, environmental impacts, and research perspectives. Particuology 85, 296–309. https://doi.org/10.1016/j.partic.2023.07.012.

Jones, F., Bankiewicz, D., Hupa, M., 2014. Occurrence and sources of zinc in fuels. Fuel 117, 763–775. https://doi.org/10.1016/j.fuel.2013.10.005.
Kaskaoutis, D.G., Grivas, G., Oikonomou, K., Tavernaraki, P., Papoutsidaki, K., Tsagkaraki, M., Stavroulas, I., Zarmpas, P., Paraskevopoulou, D., Bougiatioti, A., Liakakou, E., Gavrouzou, M., Dumka, U.C., Hatzianastassiou, N., Sciare, J., Gerasopoulos, E., Mihalopoulos, N., 2022. Impacts of severe residential wood burning on atmospheric processing, water-soluble organic aerosol and light absorption, in an inland city of Southeastern Europe. Atmos. Environ. 280, 119139. https://doi.org/10.1016/j.atmosenv.2022.119139.
Kausley, S.B., Pandit, A.B., 2010. Modelling of solid fuel stoves. Fuel 89, 782–791. https://doi.org/10.1016/j.fuel.2009.09.019.
Kelly, F.J., Fussell, J.C., 2015. Air pollution and public health: emerging hazards and improved understanding of risk. Environ. Geochem. Health 37, 631–649. https://doi.org/10.1007/s10653-015-9720-1.
Kim, B.W., Cha, W., Choi, S., Shin, J., Choi, B.S., Kim, M., 2021. Assessment of occupational exposure to indium dust for indium-tin-oxide manufacturing workers. Biomolecules 11, 1–14. https://doi.org/10.3390/biom11030419.
Kim, K.H., Kabir, E., Kabir, S., 2015. A review on the human health impact of airborne particulate matter. Environ. Int. 74, 136–143. https://doi.org/10.1016/j.envint.2014.10.005.
Klimont, Z., Kupiainen, K., Heyes, C., Purohit, P., Cofala, J., Rafaj, P., Borken-Kleefeld, J., Schöpp, W., 2017. Global anthropogenic emissions of particulate matter including black carbon. Atmos. Chem. Phys. 17, 8681–8723. https://doi.org/10.5194/acp-17-8681-2017.
Knaapen, A.M., Borm, P.J.A., Albrecht, C., Schins, R.P.F., 2004. Inhaled particles and lung cancer. Part A: mechanisms. Int. J. Cancer 109, 799–809. https://doi.org/10.1002/ijc.11708.
Kurihara, K., Iwata, A., Horwitz, S.G.M., Ogane, K., Sugioka, T., Matsuki, A., Okuda, T., 2022. Contribution of physical and chemical properties to dithiothreitol-measured oxidative potentials of atmospheric aerosol particles at urban and rural sites in Japan. Atmosphere 13 (2), 319. https://doi.org/10.3390/atmos13020319.
Kuye, A., Kumar, P., 2023. A review of the physicochemical characteristics of ultrafine particle emissions from domestic solid fuel combustion during cooking and heating. Sci. Total Environ. 886, 163747. https://doi.org/10.1016/j.scitotenv.2023.163747.
Leoni, C., Pokorná, P., Hovorka, J., Masiol, M., Topinka, J., Zhao, Y., Křůmal, K., Cliff, S., Mikuška, P., Hopke, P.K., 2018. Source apportionment of aerosol particles at a European air pollution hot spot using particle number size distributions and chemical composition. Environ. Pollut. 234, 145–154. https://doi.org/10.1016/J.ENVPOL.2017.10.097.
Li, N., Hao, M., Phalen, R.F., Hinds, W.C., Nel, A.E., 2003. Particulate air pollutants and asthma: a paradigm for the role of oxidative stress in PM-induced adverse health effects. Clin. Immunol. https://doi.org/10.1016/j.clim.2003.08.006.
Li, M., Fan, X., Zhu, M., Zou, C., Song, J., Wei, S., Jia, W., Peng, P., 2019a. Abundance and light absorption properties of brown carbon emitted from residential coal combustion in China. Environ. Sci. Technol. 53, 595–603. https://doi.org/10.1021/acs.est.8b05630.
Li, R., Han, Y., Wang, L., Shang, Y., Chen, Y., 2019b. Differences in oxidative potential of black carbon from three combustion emission sources in China. J. Environ. Manag. 240, 57–65. https://doi.org/10.1016/j.jenvman.2019.03.070.
Li, R., Yan, C., Tian, Y., Wu, Y., Zhou, R., Meng, Q., Fang, L., Yue, Y., Yang, Y., Chen, H., Yang, L., Jiang, W., 2025. Insights into relationship of oxidative potential of particles in the atmosphere and entering the human respiratory system with particle size, composition and source: a case study in a coastal area in Northern China. J. Hazard. Mater. 485, 136842. https://doi.org/10.1016/j.jhazmat.2024.136842.
Li, X., Zhang, C., Zhuo, W., Zhuo, Y., Yang, J., Song, M., Mu, Y., 2022. Significant emission reductions of carbonaceous aerosols from residential coal burning by a novel stove. J. Environ. Sci. (China) 120, 135–143. https://doi.org/10.1016/j.jes.2021.08.042.
Liang, Z., Zhou, L., Infante Cuevas, R.A., Li, X., Cheng, C., Li, M., Tang, R., Zhang, R., Lee, P.K.H., Lai, A.C.K., Chan, C.K., 2022. Sulfate formation in incense burning particles: a single-particle mass spectrometric study. Environ. Sci. Technol. Lett. 9, 718–725. https://doi.org/10.1021/acs.estlett.2c00492.
Lin, C., Ceburnis, D., Huang, R.J., Xu, W., Spohn, T., Martin, D., Buckley, P., Wenger, J., Hellebust, S., Rinaldi, M., Cristina Facchini, M., O'Dowd, C., Ovadnevaite, J., 2019. Wintertime aerosol dominated by solid-fuel-burning emissions across Ireland: insight into the spatial and chemical variation in submicron aerosol. Atmos. Chem. Phys. 19, 14091–14106. https://doi.org/10.5194/ACP-19-14091-2019.
Liu, L., Kong, S., Zhang, Y., Wang, Y., Xu, L., Yan, Q., Lingaswamy, A.P., Shi, Z., Lv, S., Niu, H., Shao, L., Hu, M., Zhang, D., Chen, J., Zhang, X., Li, W., 2017. Morphology, composition, and mixing state of primary particles from combustion sources - crop residue, wood, and solid waste. Sci. Rep. 7, 1–15. https://doi.org/10.1038/s41598-017-05357-2.
López-Caravaca, A., Crespo, J., Galindo, N., Yubero, E., Juárez, N., Nicolás, J.F., 2023. Sources of water-soluble organic carbon in fine particles at a southern European urban background site. Atmos. Environ. 306, 119844. https://doi.org/10.1016/j.atmosenv.2023.119844.
López-Caravaca, A., Vicente, E.D., Figueiredo, D., Evtyugina, M., Nicolás, J.F., Yubero, E., Galindo, N., Ryšavý, J., Alves, C.A., 2024. Gaseous and aerosol emissions from open burning of tree pruning and hedge trimming residues: detailed composition and toxicity. Atmos. Environ. 338, 120849. https://doi.org/10.1016/j.atmosenv.2024.120849.
Luo, Y., Zeng, Y., Xu, H., Li, D., Zhang, T., Lei, Y., Huang, S., 2023. Connecting oxidative potential with organic carbon molecule composition and source-specific apportionment in $PM_{2.5}$ in Xi'an, China. Atmos. Environ. 306, 119808. https://doi.org/10.1016/j.atmosenv.2023.119808.
Ma, Y., Cheng, Y., Qiu, X., Cao, G., Fang, Y., Wang, J., Zhu, T., Yu, J., 2018. Sources and oxidative potential of water-soluble humic-like substances ($HULIS_{WS}$) in fine particulate matter ($PM_{2.5}$) in Beijing. Atmos. Chem. Phys. 18, 5607–5617. https://doi.org/10.5194/acp-18-5607-2018.
Maher, B.A., Ahmed, I.A.M., Karloukovski, V., MacLaren, D.A., Foulds, P.G., Allsop, D., Mann, D.M.A., Torres-Jardón, R., Calderon-Garciduenas, L., 2016. Magnetite pollution nanoparticles in the human brain. Proc. Natl. Acad. Sci. U. S. A 113, 10797–10801. https://doi.org/10.1073/pnas.1605941113.
Martinez-Finley, E.J., Gavin, C.E., Aschner, M., Gunter, T.E., 2013. Manganese neurotoxicity and the role of reactive oxygen species. Free Radic. Biol. Med. 62, 65–75. https://doi.org/10.1016/j.freeradbiomed.2013.01.032.
Maschowski, C., Kruspan, P., Garra, P., Talib Arif, A., Trouvé, G., Gieré, R., 2019. Physicochemical and mineralogical characterization of biomass ash from different power plants in the Upper Rhine Region. Fuel 258, 116020. https://doi.org/10.1016/j.fuel.2019.116020.
Massimi, L., Frezzini, M.A., Amoroso, A., Di Giosa, A.D., Martino, L., Tiraboschi, C., Messi, M., Astolfi, M.L., Perrino, C., Canepari, S., 2024. Spatially resolved chemical data for PM_{10} and oxidative potential source apportionment in urban-industrial settings. Urban Clim. 57, 102113. https://doi.org/10.1016/j.uclim.2024.102113.
Massimi, L., Ristorini, M., Simonetti, G., Frezzini, M.A., Astolfi, M.L., Canepari, S., 2020. Spatial mapping and size distribution of oxidative potential of particulate matter released by spatially disaggregated sources. Environ. Pollut. 266, 115271. https://doi.org/10.1016/j.envpol.2020.115271.
Mayol-Bracero, O.L., Guyon, P., Graham, B., Roberts, G., Andreae, M.O., Decesari, S., Facchini, M.C., Fuzzi, S., Artaxo, P., 2002. Water-soluble organic compounds in biomass burning aerosols over Amazonia 2. Apportionment of the chemical composition and importance of the polyacidic fraction. J. Geophys. Res. Atmos. 107. https://doi.org/10.1029/2001JD000522. LBA 59-1-LBA 59-15.
Mazzoli-Rocha, F., Fernandes, S., Einicker-Lamas, M., Zin, W.A., 2010. Roles of oxidative stress in signaling and inflammation induced by particulate matter. Cell Biol. Toxicol. 26, 481–498. https://doi.org/10.1007/s10565-010-9158-2.
Molina, C., Manzano, C.A., A, R.T., G, M.A.L., 2023. The oxidative potential of airborne particulate matter in two urban areas of Chile: more than meets the eye. Environ. Int. 173, 107866. https://doi.org/10.1016/j.envint.2023.107866.
Molina, C., Toro, A.R., Manzano, C.A., Canepari, S., Massimi, L., Leiva-Guzmán, M.A., 2020. Airborne aerosols and human health: leapfrogging from mass concentration to oxidative potential. Atmosphere 11, 1–19. https://doi.org/10.3390/atmos11090917.
Mukherjee, A., Agrawal, M., 2017. World air particulate matter: sources, distribution and health effects. Environ. Chem. Lett. 15, 283–309. https://doi.org/10.1007/s10311-017-0611-9.
Nored, A.W., Shedd, J.S., Chalbot, M.C.G., Kavouras, I.G., 2022. On the role of atmospheric weathering on paint dust aerosol generated by mechanical abrasion of TiO_2 containing paints. Int. J. Environ. Res. Publ. Health 19. https://doi.org/10.3390/ijerph19031265.
Øvrevik, J., 2019. Oxidative potential versus biological effects: a review on the relevance of cell-free/abiotic assays as predictors of toxicity from airborne particulate matter. Int. J. Mol. Sci. 20. https://doi.org/10.3390/ijms20194772.
Peixoto, M.S., de Oliveira Galvão, M.F., Batistuzzo de Medeiros, S.R., 2017. Cell death pathways of particulate matter toxicity. Chemosphere 188, 32–48. https://doi.org/10.1016/j.chemosphere.2017.08.076.
Perrino, C., Pelliccioni, A., Tofful, L., Canepari, S., 2022. Indoor PM_{10} in university classrooms: chemical composition and source behaviour. Atmos. Environ. 287, 119260. https://doi.org/10.1016/j.atmosenv.2022.119260.
Pietrogrande, M.C., Bertoli, I., Clauser, G., Dalpiaz, C., Dell'Anna, R., Lazzeri, P., Lenzi, W., Russo, M., 2021. Chemical composition and oxidative potential of atmospheric particles heavily impacted by residential wood burning in the alpine region of northern Italy. Atmos. Environ. 253, 118360. https://doi.org/10.1016/j.atmosenv.2021.118360.
Ramya, C.B., Aswini, A.R., Hegde, P., Boreddy, S.K.R., Babu, S.S., 2023. Water-soluble organic aerosols over South Asia – seasonal changes and source characteristics. Sci. Total Environ. 900, 165644. https://doi.org/10.1016/j.scitotenv.2023.165644.
Rao, L., Zhang, L., Wang, X., Xie, T., Zhou, S., Lu, S., Liu, X., Lu, H., Xiao, K., Wang, W., Wang, Q., 2020. Oxidative potential induced by ambient particulate matters with acellular assays: a review. Processes 8, 1–21. https://doi.org/10.3390/pr8111410.
Schwarz, J., Pokorná, P., Rychlík, Š., Škáchová, H., Vlček, O., Smolík, J., Ždímal, V., Hůnová, I., 2019. Assessment of air pollution origin based on year-long parallel measurement of $PM_{2.5}$ and PM_{10} at two suburban sites in Prague, Czech Republic. Sci. Total Environ. 664, 1107–1116. https://doi.org/10.1016/J.SCITOTENV.2019.01.426.
Shahpoury, P., Zhang, Z.W., Arangio, A., Celo, V., Dabek-Zlotorzynska, E., Harner, T., Nenes, A., 2021. The influence of chemical composition, aerosol acidity, and metal dissolution on the oxidative potential of fine particulate matter and redox potential of the lung lining fluid. Environ. Int. 148, 106343. https://doi.org/10.1016/j.envint.2020.106343.
Shangguan, Y., Zhuang, X., Querol, X., Li, B., Moreno, N., Trechera, P., Sola, P.C., Uzu, G., Li, J., 2024. Physicochemical characteristics and oxidative potential of size-segregated respirable coal mine dust: implications for potentially hazardous agents and health risk assessment. Int. J. Coal Geol. 282. https://doi.org/10.1016/j.coal.2023.104433.
Sharma, B., Mao, J., Jia, S., Sharma, S.K., Mandal, T.K., Bau, S., Sarkar, S., 2024. Size-distribution and driving factors of aerosol oxidative potential in rural kitchen microenvironments of northeastern India. Environ. Pollut. 343, 123246. https://doi.org/10.1016/j.envpol.2023.123246.

Smołka-Danielowska, D., Jabłońska, M., Godziek, S., 2021. The influence of hard coal combustion in individual household furnaces on the atmosphere quality in Pszczyna (Poland). Minerals 11, 1155. https://doi.org/10.3390/MIN11111155.

Snyder, D.C., Rutter, A.P., Collins, R., Worley, C., Schauer, J.J., 2009. Insights into the origin of water soluble organic carbon in atmospheric fine particulate matter. Aerosol Sci. Technol. 43, 1099–1107. https://doi.org/10.1080/02786820903188701.

Timonen, H., Saarikoski, S., Tolonen-Kivimä, O., Aurela, M., Saarnio, K., Petaja, T., Aalto, P.P., Kulmala, M., Pakkanen, T., Hillamo, R., 2008. Size distributions, sources and source areas of water-soluble organic carbon in urban background air. Atmos. Chem. Phys. 8, 5635–5647. https://doi.org/10.5194/acp-8-5635-2008.

Trojanowski, R., Fthenakis, V., 2019. Nanoparticle emissions from residential wood combustion: a critical literature review, characterization, and recommendations. Renew. Sustain. Energy Rev. 103, 515–528. https://doi.org/10.1016/j.rser.2019.01.007.

Unga, F., Calzolai, G., Chiari, M., Cuccia, E., Colombi, C., Franciosa, M., Dinoi, A., Merico, E., Pennetta, A., Gómez-sánchez, N., 2025. Determination of aerosol composition by ED-XRF on Teflon and quartz substrates: potentialities and limits. Aerosol Res 3, 405–415. https://doi.org/10.5194/ar-3-405-2025.

USGS (U.S. Geological Survey), 2024. Barite-Mineral Commodity Summaries, 2024. U.S. Geological Survey, Reston, VA. https://pubs.usgs.gov (accessed September 2, 2025).

Utinger, B., Barth, A., Paul, A., Mukherjee, A., Campbell, S.J., 2025. Emission dynamics of reactive oxygen species and oxidative potential in particles from a petrol car and wood stove. Aerosol Res 3, 205–218. https://doi.org/10.5194/ar-3-205-2025.

Vaccarella, E., Massimi, L., Canepari, S., 2025. Assessment of oxidative stress induced by atmospheric particulate matter: from acellular and cellular assays to the use of model and experimental organisms. Sci. Total Environ. 965, 178651. https://doi.org/10.1016/j.scitotenv.2025.178651.

Vassilev, S.V., Baxter, D., Andersen, L.K., Vassileva, C.G., 2010. An overview of the chemical composition of biomass. Fuel 89, 913–933. https://doi.org/10.1016/j.fuel.2009.10.022.

Verma, V., Fang, T., Xu, L., Peltier, R.E., Russell, A.G., Ng, N.L., Weber, R.J., 2015. Organic aerosols associated with the generation of reactive oxygen species (ROS) by water-soluble $PM_{2.5}$. Environ. Sci. Technol. 49, 4646–4656. https://doi.org/10.1021/es505577w.

Verma, V., Rico-Martinez, R., Kotra, N., King, L., Liu, J., Snell, T.W., Weber, R.J., 2012. Contribution of water-soluble and insoluble components and their hydrophobic/hydrophilic subfractions to the reactive oxygen species-generating potential of fine ambient aerosols. Environ. Sci. Technol. 46, 11384–11392. https://doi.org/10.1021/es302484r.

Vicente, E., Calvo, A.I., Sainnokhoi, T.A., Kováts, N., de la Campa, A.S., de la Rosa, J., Oduber, F., Nunes, T., Fraile, R., Tomé, M., Alves, C.A., 2024a. Indoor PM from residential coal combustion: levels, chemical composition, and toxicity. Sci. Total Environ. 918, 170598. https://doi.org/10.1016/j.scitotenv.2024.170598.

Vicente, E.D., Alves, C.A., 2018. An overview of particulate emissions from residential biomass combustion. Atmos. Res. 199, 159–185. https://doi.org/10.1016/j.atmosres.2017.08.027.

Vicente, E.D., Vicente, A.M., Evtyugina, M., Oduber, F.I., Amato, F., Querol, X., Alves, C., 2020. Impact of wood combustion on indoor air quality. Sci. Total Environ. 705, 135769. https://doi.org/10.1016/j.scitotenv.2019.135769.

Vicente, Figueiredo, D., Alves, C., 2024b. Toxicity of particulate emissions from residential biomass combustion: an overview of *in vitro* studies using cell models. Sci. Total Environ. 927, 171999. https://doi.org/10.1016/j.scitotenv.2024.171999.

Wang, Y., Plewa, M.J., Mukherjee, U.K., Verma, V., 2018. Assessing the cytotoxicity of ambient particulate matter (PM) using Chinese hamster ovary (CHO) cells and its relationship with the PM chemical composition and oxidative potential. Atmos. Environ. 179, 132–141. https://doi.org/10.1016/j.atmosenv.2018.02.025.

Waring, M.S., 2014. Secondary organic aerosol in residences: predicting its fraction of fine particle mass and determinants of formation strength. Indoor Air 24, 376–389. https://doi.org/10.1111/ina.12092.

Weagle, C.L., Snider, G., Li, C., Van Donkelaar, A., Philip, S., Bissonnette, P., Burke, J., Jackson, J., Latimer, R., Stone, E., Abboud, I., Akoshile, C., Anh, N.X., Brook, J.R., Cohen, A., Dong, J., Gibson, M.D., Griffith, D., He, K.B., Holben, B.N., Kahn, R., Keller, C.A., Kim, J.S., Lagrosas, N., Lestari, P., Khian, Y.L., Liu, Y., Marais, E.A., Martins, J.V., Misra, A., Muliane, U., Pratiwi, R., Quel, E.J., Salam, A., Segev, L., Tripathi, S.N., Wang, C., Zhang, Q., Brauer, M., Rudich, Y., Martin, R.V., 2018. Global sources of fine particulate matter: interpretation of $PM_{2.5}$ chemical composition observed by SPARTAN using a global chemical transport model. Environ. Sci. Technol. 52, 11670–11681. https://doi.org/10.1021/acs.est.8b01658.

Weber, S., Uzu, G., Favez, O., Borlaza, L.J.S., Calas, A., Salameh, D., Chevrier, F., Allard, J., Besombes, J., Albinet, A., Pontet, S., Mesbah, B., Blanc, U.M., Auvergne-rhône-alpes, A., Sud, A., Est, A.G., 2021. Source apportionment of atmospheric PM_{10} oxidative potential: synthesis of 15 year-round urban datasets in France. Atmos. Chem. Phys. 21, 11353–11378. https://doi.org/10.5194/acp-21-11353-2021.

Wen, J., Shi, G., Tian, Y., Chen, G., Liu, J., Huang-Fu, Y., Ivey, C.E., Feng, Y., 2018. Source contributions to water-soluble organic carbon and water-insoluble organic carbon in $PM_{2.5}$ during Spring Festival, heating and non-heating seasons. Ecotoxicol. Environ. Saf. 164, 172–180. https://doi.org/10.1016/j.ecoenv.2018.08.002.

Wolf, T., Pettersson, L.H., Esau, I., 2021. Dispersion of particulate matter ($PM_{2.5}$) from wood combustion for residential heating: optimization of mitigation actions based on large-eddy simulations. Atmos. Chem. Phys. 21, 12463–12477. https://doi.org/10.5194/acp-21-12463-2021.

Wu, G., Zhang, X., Zhang, C., Xu, T., 2016. Mineralogical and morphological properties of individual dust particles in ice cores from the Tibetan Plateau. J. Glaciol. 62, 46–53. https://doi.org/10.1017/jog.2016.8.

Xu, M., Yan, R., Zheng, C., Qiao, Y., Han, J., Sheng, C., 2004. Status of trace element emission in a coal combustion process: a review. Fuel Process. Technol. 85, 215–237. https://doi.org/10.1016/S0378-3820(03)00174-7.

Xu, W., Chen, X., Liu, D., Jiang, W., Yang, B., 2023. Systematic thermodynamic and experimental studies for recovering indium and tin from indium tin oxide waste target with hydrogen. J. Clean. Prod. 429, 139328. https://doi.org/10.1016/j.jclepro.2023.139328.

Yang, Y., Battaglia, M.A., Robinson, E.S., DeCarlo, P.F., Edwards, K.C., Fang, T., Kapur, S., Shiraiwa, M., Cesler-Maloney, M., Simpson, W.R., Campbell, J.R., Nenes, A., Mao, J., Weber, R.J., 2024. Indoor–outdoor oxidative potential of $PM_{2.5}$ in wintertime Fairbanks, Alaska: impact of air infiltration and indoor activities. ACS ES&T Air 1, 188–199. https://doi.org/10.1021/acsestair.3c00067.

Yu, H., Puthussery, J.V., Wang, Y., Verma, V., 2021. Spatiotemporal variability in the oxidative potential of ambient fine particulate matter in the Midwestern United States. Atmos. Chem. Phys. 21, 16363–16386. https://doi.org/10.5194/acp-21-16363-2021.

Yu, H., Wang, Y., Puthussery, J.V., Verma, V., 2024. Sources of acellular oxidative potential of water-soluble fine ambient particulate matter in the midwestern United States. J. Hazard. Mater. 474, 134763. https://doi.org/10.1016/j.jhazmat.2024.134763.

Zhang, J., Qi, A., Wang, Q., Huang, Q., Yao, S., Li, J., Yu, H., Yang, L., 2022. Characteristics of water-soluble organic carbon (WSOC) in $PM_{2.5}$ in inland and coastal cities. China. Atmos. Pollut. Res. 13, 101447. https://doi.org/10.1016/j.apr.2022.101447.

Zhang, L., Li, J., Li, Y., Liu, X., Luo, Z., Shen, G., Tao, S., 2024a. Comparison of water-soluble and water-insoluble organic compositions attributing to different light absorption efficiency between residential coal and biomass burning emissions. Atmos. Chem. Phys. 24, 6323–6337. https://doi.org/10.5194/acp-24-6323-2024.

Zhang, L., Li, Y., Li, J., Xing, R., Liu, X., Zhao, J., Shen, G., Pan, B., Li, X., Tao, S., 2024b. Pollutant emissions and oxidative potentials of particles from the indoor burning of biomass pellets. Environ. Sci. Technol. 58, 16016–16027. https://doi.org/10.1021/acs.est.4c03967.

Zhang, Y., Yuan, Q., Huang, D., Kong, S., Zhang, J., Wang, X., Lu, C., Shi, Z., Zhang, X., Sun, Y., Wang, Z., Shao, L., Zhu, J., Li, W., 2018. Direct observations of fine primary particles from residential coal burning: insights into their morphology, composition, and hygroscopicity. J. Geophys. Res. Atmos. 123 (12), 964. https://doi.org/10.1029/2018JD028988, 12,979.